Selective inhibition in CA3: A mechanism for stable pattern completion through heterosynaptic plasticity

Gyeongtae Kim
Department of Mathematical Sciences
Ulsan National Institute of Science and Technology (UNIST)
Ulsan, Republic of Korea
kgt1220@unist.ac.kr

Pilwon Kim*
Department of Mathematical Sciences
Ulsan National Institute of Science and Technology (UNIST)
Ulsan, Republic of Korea
pwkim@unist.ac.kr

August 16, 2024

ABSTRACT

Engrams compete for successful retrieval in the CA3 of the hippocampus, but the detailed mechanisms of their formation remain elusive. Recent research reveals that hippocampal inhibitory neurons respond selectively to stimuli and exhibit diverse plasticity, implying their significance in engram formation. Conventional attractor network models for CA3 commonly employ global inhibition where inhibitory neurons uniformly reduce the activation of excitatory neurons. However, these models may not fully capture the diverse competition conditions arising from sparse distributed coding and not accurately reflect the specific roles of inhibitory neurons in engram competition. We propose an engram formation mechanism in CA3, highlighting the critical role of the association between excitatory and inhibitory neurons through heterosynaptic plasticity. In the proposed model, an inhibitory neuron is associated with specific neural assemblies and it selectively inhibits the excitatory neurons for retrieval that belong to competing assemblies. With a simplified dentate gyrus (DG) in a feed-forward structure, this proposed mechanism results in sparsely distributed engrams in CA3. The sparse distributed coding implemented in the model allows us to investigate the effects of selective inhibition on pattern completion under various configurations, such as partially overlapping competing engrams. Our results show that selective inhibition leads to more stable and improved retrieval performance than global inhibition alone. We observed the neural activities of the hippocampal subregions in the model for pattern separation and pattern completion, aligning with experimental findings on their respective roles.

1 Introduction

The hippocampus is a crucial region for processing episodic memory [O'Keefe and Nadel, 1978, Tulving, 1983]. Within this region, engrams—neural circuits representing the physical trace of a memory—are stored and retrieved [Semon et al., 1923, Josselyn and Tonegawa, 2020]. Specifically, engrams are sparsely and distributedly formed in CA3, facilitated by sparse activations from the DG [Wixted et al., 2014]. This mechanism, known as pattern separation, functions to create distinct and non-overlapping representations of similar events or stimuli. It is one of the key functions of the hippocampus, which reduces interference between memories [Marr, 1971, McClelland et al., 1995, Berron et al., 2016, Rolls, 2016, Knierim and Neunuebel, 2016]. Successful pattern separation is achieved when distinct representations in CA3 are formed regardless of similarities in external information. [Leutgeb et al., 2007, Treves et al.,

2008, Yassa and Stark, 2011, Santoro, 2013].
While engrams are sparsely and distributedly represented in CA3, the hippocampus can retrieve specific memories based on the characteristics of the encoded information. This process, reconstruction of a complete memory from partial or incomplete cues, is called pattern completion [Marr, 1971, McClelland et al., 1995, Norman and O'Reilly, 2003, Lee et al., 2004, Rolls, 2016, Knierim and Neunuebel, 2016, Guzman et al., 2016]. It relies on two critical hippocampal pathways: the direct perforant path (PP) from the entorhinal cortex(EC) to CA3 and the recurrent collateral (Rc) within CA3. The direct PP encodes characteristics of information, enabling neural assemblies in CA3 to respond to similarities between cues and stored memories. Then, Rc activates neurons within the assemblies to facilitate pattern completion.
Although the processes of pattern separation and pattern completion in the hippocampus are well understood, understanding how engrams in CA3 are formed remains elusive, particularly concerning the role of inhibitory neurons in these processes. Attractor network models describe pattern completion in CA3 within the context of engram competition [Hopfield, 1982, Káli and Dayan, 2000, Rolls, 2007, Rennó-Costa et al., 2014], but they do not specifically deal with the mechanisms underlying the formation of the engram. Most of these models assume completely separated engrams that compete through a winner-takes-all process. They commonly use global inhibition for competition where inhibitory neurons uniformly suppress all excitatory neurons.
Recent research has highlighted the crucial role of inhibitory neurons in the memory process [Raven and Aton, 2021, Cummings et al., 2021]. Stimulus-selectivity was primarily associated with excitatory neurons [Usrey et al., 2003, Niell and Stryker, 2008]; however, recent studies reveal that many GABAergic neurons exhibit greater stimulus-selectivity than previously recognized [Li et al., 2014, Khan et al., 2018]. In addition, increasing evidence shows the presence of synaptic plasticity mechanisms in inhibitory neurons. Both long-term potentiation (LTP) and long-term depression (LTD) have been observed at inhibitory neuron synapses, as previously observed at excitatory neurons [Perez et al., 2001, Owen et al., 2013, Cohen et al., 2016, Korotkova et al., 2010, He et al., 2021]. This plasticity contributes to engram formation and refinement by modulating inhibitory control based on experience. These observations suggest an extended role for inhibitory neurons in memory encoding, storage, and retrieval processes, beyond their contribution to sparse distributed coding [Acsády et al., 1998, Rolls, 2013].
Building on the body of evidence presented above, our work aims to explore the roles of inhibitory neurons in pattern completion through a modeling approach. We propose that inhibitory neurons can offer functional advantages by providing selective inhibition in engram competition beyond the effects of global inhibition, potentially enhancing the stability and efficiency of this process. We developed a spiking neural network model that preserves structural and connectional properties of the hippocampus, focusing on the trisynaptic circuit—the pathway to CA3 from the EC via DG. Drawing from the evidence of heterosynaptic plasticity observed in various connections [Tsukamoto et al., 2003, Hunt et al., 2013, Chater and Goda, 2021, Jenks et al., 2021], we propose a mechanism of engram formation in which heterosynaptic plasticity between excitatory and inhibitory neurons in CA3 naturally induces selective inhibition for engram competition.
Selective inhibition in the proposed model is characterized by inhibitory neurons associated with a particular neural assembly in CA3: they inhibit excitatory neurons in competing assemblies, except for the excitatory neurons within the same assembly. To investigate the effect of selective inhibition on pattern completion, we simplified the DG into a feed-forward structure. This simplification facilitates instant sparse distributed coding and creates various competitive conditions in conjunction with our proposed mechanism of engram formation. It gives rise to configurations for engram competition in CA3, such as multiple overlapped engrams of various sizes.
We conducted pattern separation and pattern completion tasks across the entire hippocampal model, leveraging the stable retrieval performance. The resulting activation patterns in each subregion were then compared with experimental data. Our analysis shows that selective inhibition by inhibitory neurons enhances the stability and efficiency of engram competition. These results provide novel insights into the role of inhibitory neurons in pattern completion and separation within the hippocampus.

2 Results

2.1 Model architecture and learning mechanisms

We constructed a spiking neural network that preserves the hippocampal structure to describe the CA3 engram formation process and competition between them for retrieval ('Materials and methods'). The model focuses on investigating the stability of pattern completion under various conditions. To achieve this, engrams in CA3 should be naturally formed for arbitrary inputs via the DG, resulting in a sparse distributed representation. However, modeling DG pattern separation is challenging due to its intricate circuitry, synaptic connectivity, and the heterogeneity of neuronal types [Jinde et al., 2013, Cayco-Gajic et al., 2017, Hainmueller and Bartos, 2020]. Therefore, we simplified our approach by focusing solely on spatial pattern separation for non-sequential inputs, represented as binary vectors in 16 dimensions, at a fixed frequency ('Materials and methods'). Under these conditions, we designed a feedforward form of the DG, which we will explain in more detail in the next section 'Feedforward form of the dentate gyrus and its inherent ability

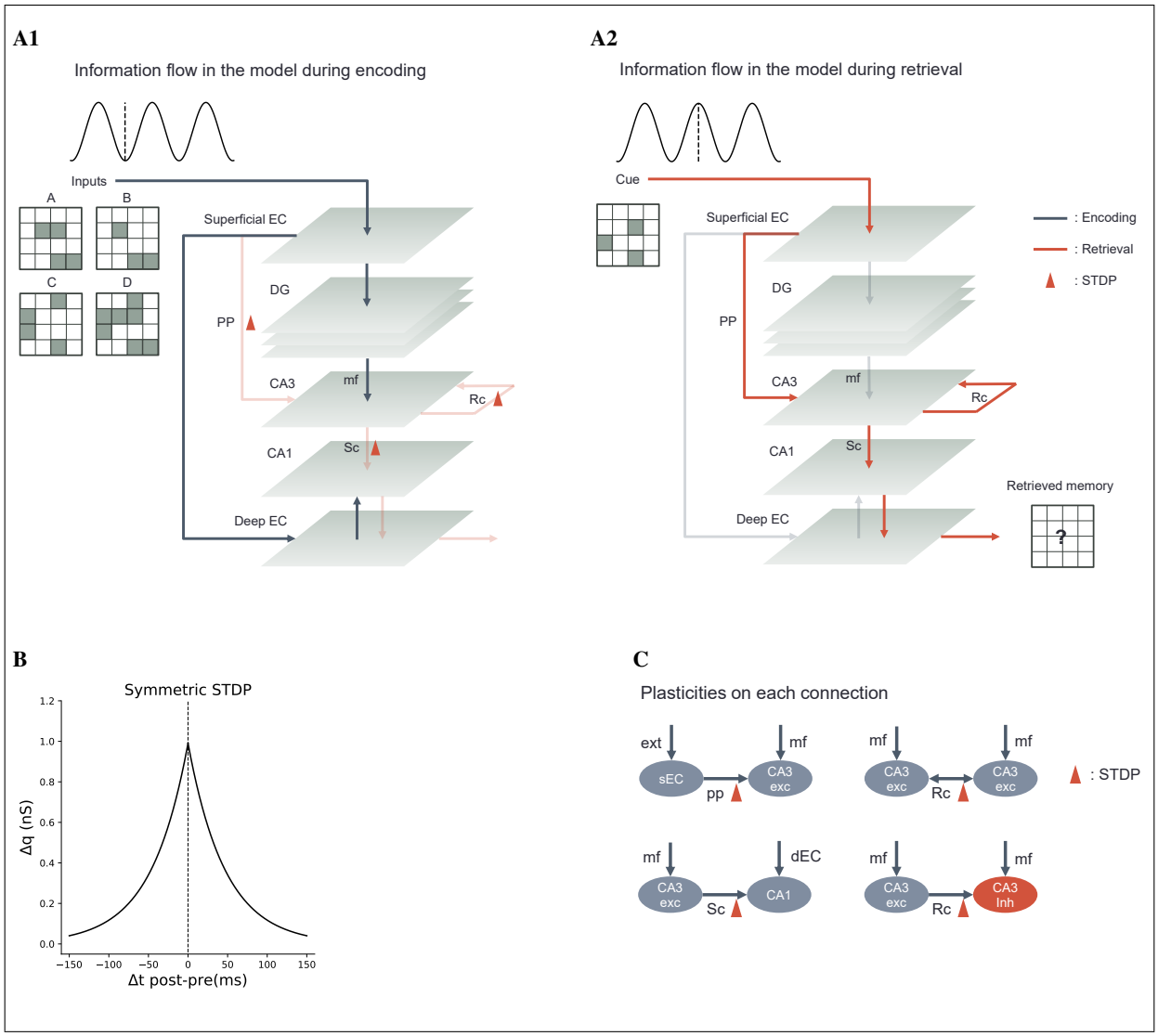

Figure 1: Overview of model architecture and learning. **(A)** The model consists of the hippocampus subfields: DG, CA3, and CA1, and superficial and deep layers of the EC. The model features two distinct phases based on theta oscillations, where encoding and retrieval are processed separately. **(A1)** Information flow during the encoding phase. superficial EC sends inputs to DG and deep EC, but not CA3 directly. Synaptic plasticity occurs at the silenced connections during the encoding phase, perforant path (pp) from superficial EC to CA3, Rc, and Schaffer collateral(Sc). **(A2)** Information flow during the retrieval phase. The superficial EC sends inputs directly to CA3, retrieving memories in the deep EC via Rc, Sc, and CA1. **(B)** Symmetric spike-timing-dependent plasticity (STDP) kernel used in the encoding phase. **(C)** Synaptic plasticity on various connections. ext: external input; mf: mossy fiber; exc: excitatory neuron; inh: inhibitory neuron.

for spatial pattern separation.

Additionally, we simplified CA1's role to reinstating original information from CA3 engrams ('Materials and methods'). All neurons in the network were modeled using the Izhichevich model [Izhikevich and Edelman, 2008], where we distinguished various types of hippocampal neurons as either excitatory or inhibitory neurons ('Materials and methods'). The model operates in different phases based on the theta oscillation theory [Hasselmo and Stern, 2014]. Theta oscillations, rhythmic brain waves typically in the 4-8 Hz range, are prominent in the hippocampus and are crucial for memory processes Various theories have been proposed to explain the specific functions of theta waves [Hasselmo and Stern, 2014, Drieu and Zugaro, 2019, Herweg et al., 2020]. One suggests that theta oscillations divide information processing into discrete time windows, optimizing memory processing by coordinating information flow across different hippocampal subregions [Bragin et al., 1995, Colgin, 2016, dos Santos et al., 2018, Kragel et al., 2020, Reddy et al.,

2021, Ter Wal et al., 2021, Lowet et al., 2023, Gattas et al., 2023].
During the encoding phase, the superficial entorhinal cortex (EC) sends inputs to CA3 via the DG and to the deep EC, which subsequently sends inputs to CA1 (Figure 1A1). Four types of connections—direct PP, Rc, Schaffer collateral (Sc), and connection to deep EC from CA1—are silenced yet undergo learning through heterosynaptic plasticity, except for the connection to deep EC (Figure 1C). We applied symmetric spike-timing-dependent plasticity (STDP) in the model for simplicity, despite various studies on STDP dynamics for each connection type ('Material and methods' and Figure 1B) [Wittenberg and Wang, 2006, Mishra et al., 2016, Rebola et al., 2017, Ecker et al., 2022].
During the retrieval phase, all of the connections that were silenced during the encoding phase are activated, while the connections that were active during the encoding phase are silenced. The superficial EC sends inputs to CA3 via the direct PP, where engram competition occurs, resulting in pattern completion. The winning engram in CA3 activates CA1, which in turn triggers the neurons in the deep EC (Figure 1A2). Each phase is given 120 ms, which is sufficient time to store information and observe retrieval. Since there is no interaction between the encoding and retrieval phases in the model, we did not coordinate the encoding and retrieval phases with oscillatory cycles for most tasks, nor did we base the generation of oscillations on biological processes such as those in the medial septum [Cheng and Yakel, 2015, Robinson et al., 2016, Unal et al., 2018, Müller and Remy, 2018, Nuñez and Buño, 2021, Gedankien et al., 2023]. We focused primarily on the distinct information flows for each phase to simplify the model.

2.2 Engram formation with selective inhibition through heterosynaptic plasticity

This section details the mechanism of engram formation in the model, emphasizing the novel role of selective inhibition mediated by heterosynaptic plasticity. Mossy fibers from the DG project to both pyramidal neurons and inhibitory neurons in the CA3 region, facilitating sparse distributed coding [Acsády et al., 1998, Mori et al., 2007, Torborg et al., 2010, Treviño et al., 2011, Cosgrove et al., 2010, Prince et al., 2016]. These fibers transmit the outputs of pattern separation performed by the DG. We focused particularly on mossy fiber inputs to inhibitory neurons in CA3 due to their involvement in feedforward inhibition, which regulates pyramidal neuron activity [Ruediger et al., 2011, Morrison et al., 2016, Stefanelli et al., 2016, Guo et al., 2018, Viana da Silva et al., 2019, Josselyn and Tonegawa, 2020, Giorgi and Marinelli, 2021]. Our hypothesis goes beyond the conventional view of feedforward inhibition as merely a sparsification mechanism. We propose that it also facilitates selective inhibition for engram competition through heterosynaptic plasticity.
Heterosynaptic plasticity, where synaptic changes in one set of synapses influence another set, is well-documented [Tsukamoto et al., 2003, Hunt et al., 2013, Chater and Goda, 2021, Jenks et al., 2021]. This form of plasticity occurs when the strength of a synapse changes due to activity at a different, nearby synapse. For example, the activation of one synapse might lead to the strengthening or weakening of neighboring synapses, even if those synapses were not directly activated. This mechanism enables more complex forms of learning compared to traditional Hebbian plasticity. Multiple studies have shown that heterosynaptic plasticity occurs in the direct PP, Rc, and Sc [Tsukamoto et al., 2003, Hunt et al., 2013, Chater and Goda, 2021, Jenks et al., 2021]. Building on this evidence, the model implements heterosynaptic plasticity at each type of connection (Figure 1C).
During the encoding phase, the inhibitory neurons suppress most of the excitatory neurons. The remaining excitatory and activated inhibitory neurons form a neural assembly through heterosynaptic plasticity (Figure 2A). In addition, these remaining excitatory neurons form associations with activated neurons in the superficial EC and CA1 through strengthened direct PP and SC connections, respectively. All of these strengthened connections lead to engram formation (Figure 1A2).
The proposed learning mechanism ensures that inhibitory neurons within an engram do not inhibit the excitatory neurons of the same engram (Figure 2C). However, inhibitory neurons are not confined to a single engram; instead, they exhibit stimulus-selectivity, corresponding with recent findings that they can show selective responses to stimuli [Li et al., 2014, Khan et al., 2018, Cummings et al., 2021]. We investigated the information storage capacity of each CA3 neuron by examining the amount of information retained after encoding 500 arbitrary inputs. As shown in Figure 2B, most excitatory neurons in CA3 (approximately 85%) store only one or two pieces of information. In contrast, inhibitory neurons have a broader range of storage capacities, with some storing more information. These results indicate that selective inhibition does not constrain the information selectivity of inhibitory neurons.
We also investigated how the overlap between CA3 engrams, involving shared excitatory neurons within CA3, affects selective inhibition. To evaluate this, we measured the ratio of suppressed excitatory neurons in each neural assembly caused by inhibitory neurons associated with another assembly. This made it possible to assess the extent to which one engram inhibits others. We prepared 500 engrams in CA3 corresponding to 500 inputs. Engrams in each pair were selected based on their overlap ratio ('Materials and methods'), and we divided the overlap ratio into 25 windows, each representing a 4% interval. The inhibition ratio was then averaged within each window. Figure 2D shows that the inhibition power of an engram over other engrams decreases as the overlap ratio between engrams increases, suggesting that selective inhibition power is reduced with higher overlap. This observation may underscore the importance of sparse distributed coding in CA3 [Marr, 1971, McClelland et al., 1995, Norman and O'Reilly, 2003, Rolls, 2016,

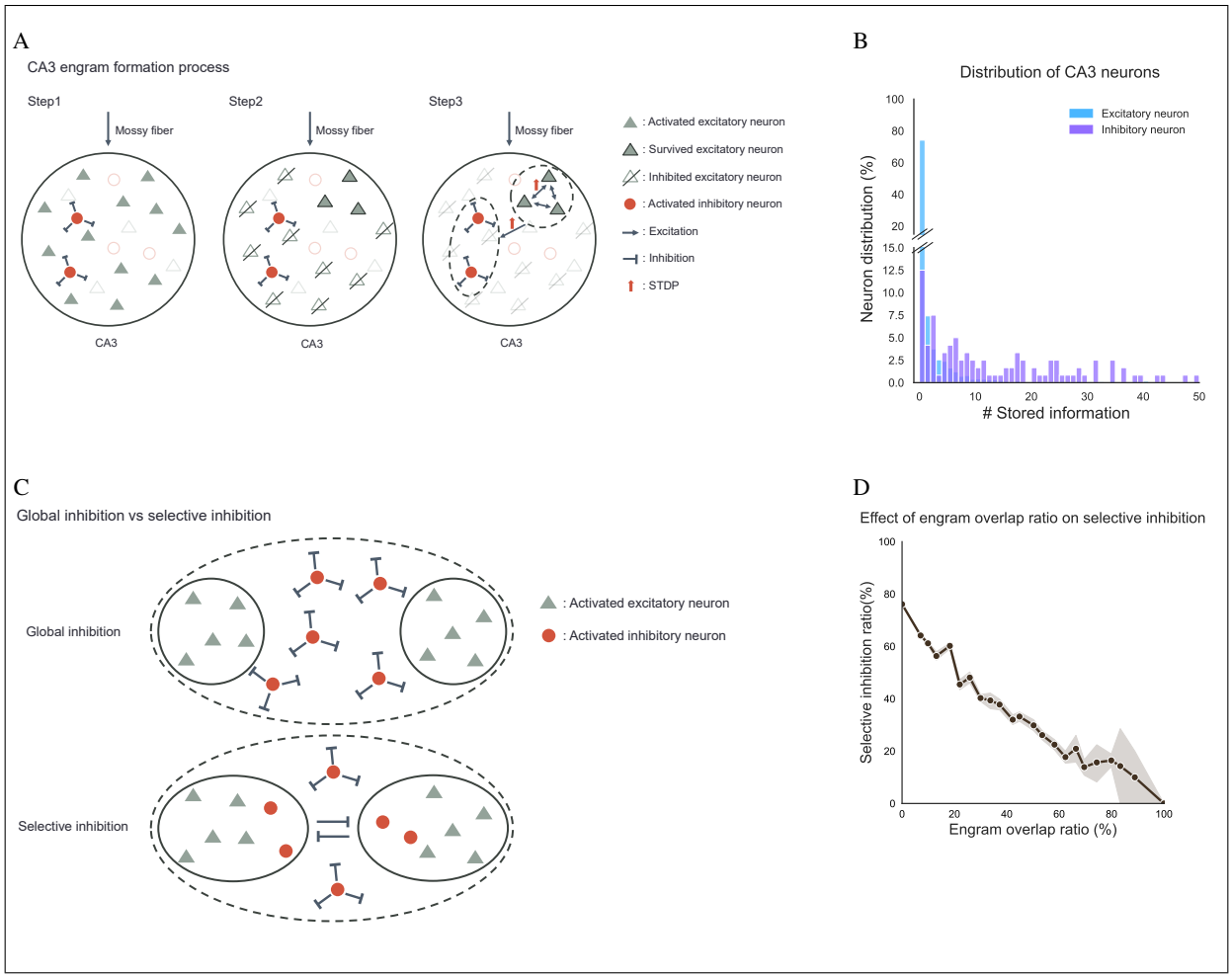

Figure 2: Illustrations and properties for selective inhibition. **(A)** Engram formation process in CA3 conferring the selective inhibition to the formed engram. Inhibitory neurons activated by mossy fibers inhibit most of the excitatory neurons. The surviving excitatory neurons form an assembly along with the activated inhibitory neurons through STDP. **(B)** Distribution of CA3 neurons over the number of stored information. **(C)** Characterization of CA3 connections with inhibitory neurons for global and selective inhibition, respectively. For global inhibition, inhibitory neurons inhibit regardless of the type of engrams. However, inhibitory neurons in the engram do not inhibit the excitatory neurons belonging to the same engram for selective inhibition. **(D)** The inhibition power of engram to other engrams over the degree of overlap between engrams.

Knierim and Neunuebel, 2016, Guzman et al., 2016].
The strengthened connections from excitatory to inhibitory neurons enable earlier activation of inhibitory neurons during retrieval. These activated inhibitory neurons then inhibit most excitatory neurons except those within the same neural assemblies in CA3, effectively guiding the retrieval cue toward a single memory. Since we initialized the connection weights to inhibitory neurons from excitatory neurons as nonzero ('Materials and methods' and Figure 5A3), global inhibition becomes effective after sufficient neurons in one assembly have started firing.
We propose that selective inhibition provides targeted suppression of competing engrams, while global inhibition helps maintain overall network stability. This inhibition mechanism potentially leads to more accurate pattern completion and reduced interference between memories having similar information. To demonstrate the stability of pattern completion with selective inhibition under natural conditions, we first need to construct a DG model that generates engrams in CA3 with various characteristics. This model will facilitate a comprehensive evaluation of our inhibition mechanism in diverse scenarios of engram competition. The following section will detail the construction of this DG model and assess its performance in sparse distributed coding through pattern separation.

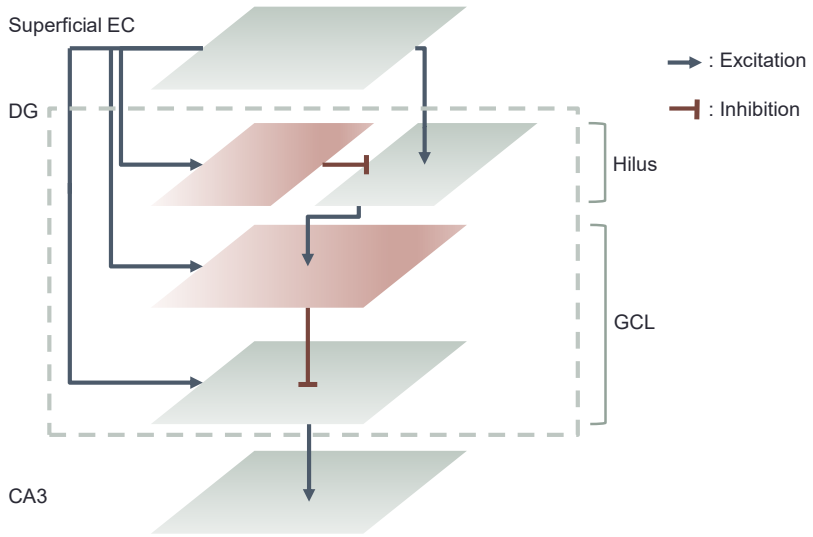

Figure 3: Dentate gyrus structure in the model. DG has a feedforward structure which consists of the Hilus layer and GCL. Both layers have excitatory neurons and inhibitory neurons: The gray color of the layers expresses excitatory neurons and the red color of the layers expresses inhibitory neurons. Superficial EC sends inputs to all types of neurons in DG. Inhibitory neurons in GCL also receive inputs from excitatory neurons in the Hilus layer, which is controlled by inhibitory neurons in the Hilus layer. Lastly, the excitatory neurons in GCL controlled by inhibitory neurons in GCL send inputs to CA3 by mossy fiber.

2.3 Feedforward form of the dentate gyrus and its inherent ability for spatial pattern separation

To equip the DG with spatial pattern separation capabilities, we modeled its structure based on the real anatomical features. We excluded the recurrent circuits, creating a feedforward configuration. Numerous modeling studies have demonstrated the pattern separation performance of the DG [Myers and Scharfman, 2009, Faghihi and Moustafa, 2015, Chavlis et al., 2017, Cayco-Gajic et al., 2017, Madar et al., 2019, Modhej et al., 2020, Guzman et al., 2021, Kim and Lim, 2022], and it is established that a feedforward DG can achieve this function [Cayco-Gajic et al., 2017]. In the model, the DG consists of two distinct layers: the Hilus layer and the granule cell layer (GCL) (Figure 3). Although the real DG contains various neuron types in each layer, such as hilar interneurons, mossy cells, basket cells, and granule cells [Freund and Buzsáki, 1996, Amaral et al., 2007, Danielson et al., 2017, Hainmueller and Bartos, 2020], we simplified these into excitatory and inhibitory neurons using the Izhikevich neuron model ('Materials and Methods'). Therefore, each layer includes both excitatory and inhibitory neurons (Figure 3).

During the encoding phase, inhibitory neurons in the GCL receive two types of excitatory inputs: direct excitation from the superficial EC and excitation from the Hilus layer. The latter is modulated by inhibitory neurons within the Hilus layer, known to play an important role in pattern separation through the disynaptic effect [Kim and Lim, 2022]. Both inputs detect features of the given input pattern, activating the inhibitory neurons in the GCL for most input patterns (Figures 3 and 4A). The excitatory neurons in the GCL become active when they simultaneously escape inhibition from GCL inhibitory neurons and receive excitatory input from the superficial EC. This mechanism transforms low-dimensional information into very sparse, high-dimensional information. The resulting activation patterns of excitatory neurons in the GCL stimulate both excitatory and inhibitory neurons in CA3 via mossy fibers, creating sparse distributed representations. We passed 10 arbitrary inputs to the DG and Figure 4A shows how these inputs are separated within the excitatory neuron population in the GCL.

To evaluate the pattern separation performance of our DG model, we presented 1000 input patterns and observed the activation patterns of excitatory neurons in the GCL. We calculated the overlap degree for each pair of patterns using the measure suggested by Löffler and Gupta [2022] and the discrimination value is defined as one minus the overlap value ('Materials and Methods'). The output discrimination values are averaged within each of the 25 windows, with each window spanning 0.04 units (Figure 4B). This figure shows that the output discrimination values rapidly approach 1.0 when input discrimination values exceed approximately 0.1. This indicates effective pattern separation, with high output discrimination maintained for input values above this point. Figure 4C illustrates the distribution of input and output pairs based on their similarity, comparing input pairs from the superficial EC and output pairs from the DG. The analysis indicates that a significant majority of input pairs (over 85%) are entirely separated, as reflected by the high

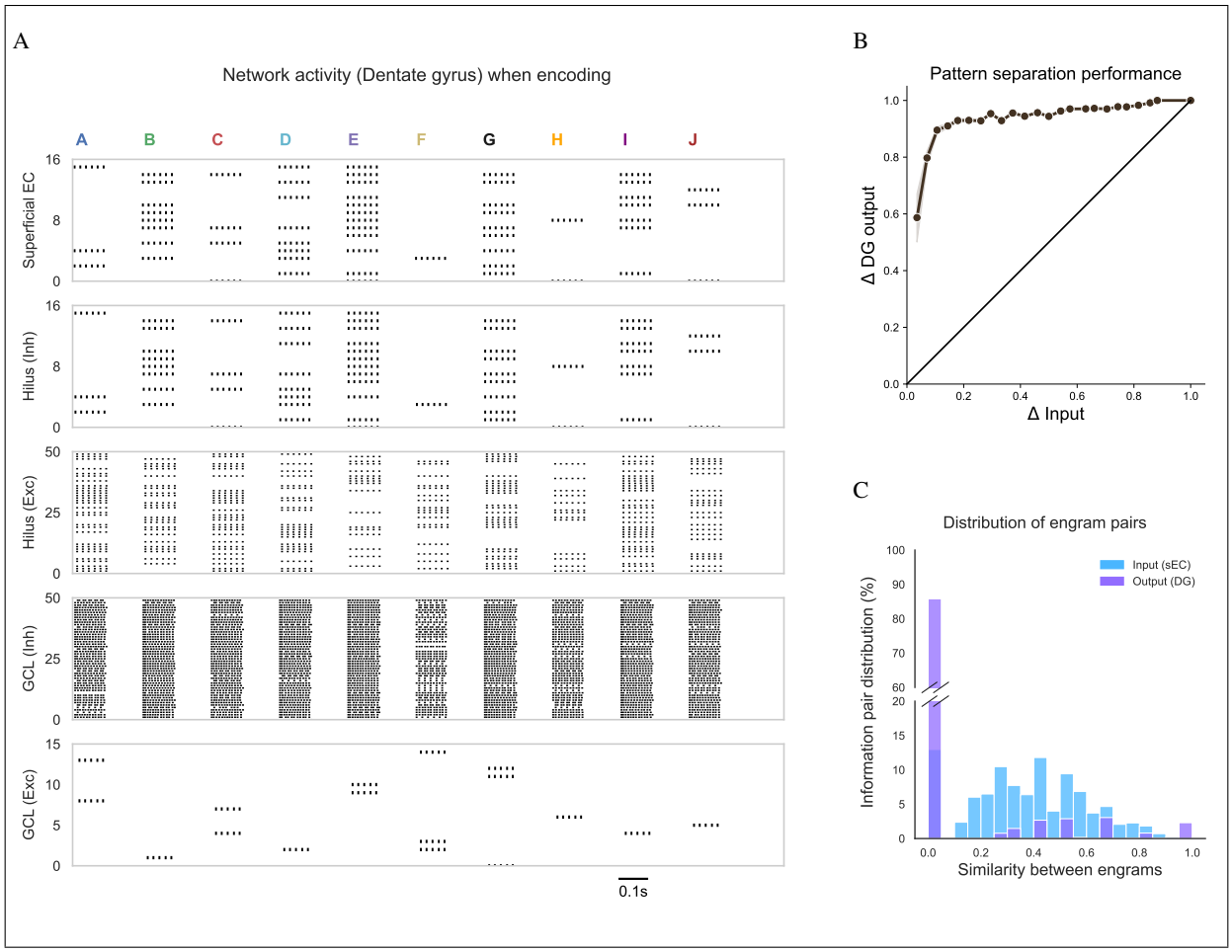

Figure 4: DG spike raster and pattern separation performance. **(A)** Raster plot showing DG activity when encoding 10 different inputs (A to J). The activity is depicted for different regions including superficial EC, excitatory and inhibitory neurons in the Hilus layer, and excitatory and inhibitory neurons in GCL. For better visualization, arbitrarily 50 neurons are selected from excitatory neurons in the Hilus and inhibitory neurons in GCL among actual 100 and 400 neurons respectively, and 16 excitatory neurons in GCL (a total of 800 neurons) involved in 10 examples of information are selected. **(B)** Pattern separation performance of DG. The graph plots the separation performance against the input similarity. **(C)** Distribution of engram pairs based on similarity for the superficial EC (input) and excitatory neurons in GCL of DG (output) respectively, showing that most of the pairs are separated by DG.

percentage of output pairs with minimal similarity. Both Figures 4B and 4C highlight the DG's spatial pattern separation ability in the model, indicating that a feedforward form is sufficient for this function even without any learning.

2.4 Sparse distributed coding for memory storage and retrieval

The proposed model, equipped with a feedforward structure of the DG, successfully separates patterns and projects inputs into a high-dimensional space. It contributes to the sparse distributed representation of memories in CA3, enabling a diverse range of neural assembly sizes and the relations among assemblies. First, we assessed the storage capacity of the CA3 region in the model to ensure it has sufficient capacity for investigating the stability of pattern completion. This was done by examining the number of distinct engrams formed in CA3 relative to the number of inputs (Figure 5C). The graph demonstrates a consistent and steady increase in the number of engrams within CA3 as the number of inputs grows. This capacity is enough to investigate the stability of selective inhibition for pattern completion.

Additionally, we analyzed the correlation between the size of the input and the size of the neural assembly in CA3 for the input patterns. The size of the patterns in each subregion is defined as the number of firing neurons in the superficial EC and CA3 regions respectively. Figure 5D shows no correlation between input size and neural assembly size in CA3,

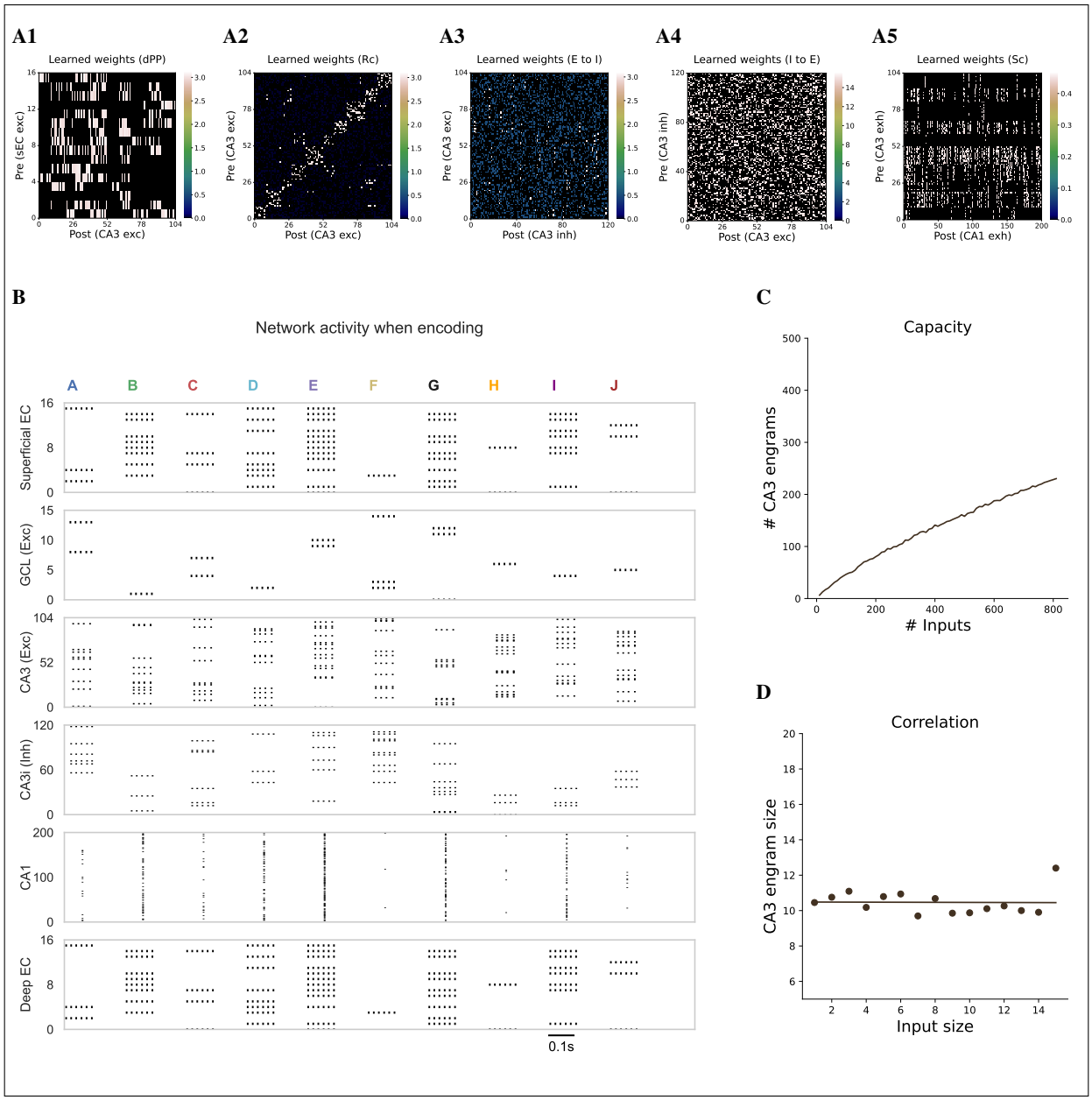

Figure 5: Encoding the various inputs. **(A)** Learned matrices by STDP during encoding. Weights mean the fixed connection weights multiplied by the learned peak conductances. The number of CA3 excitatory neurons is 2400, but we selected and arranged only CA3 neurons involved in 10 examples of information for visualization. **(A1)** Learned direct PP weight matrix for superficial EC neurons to CA3 excitatory neurons. **(A2)** Learned excitatory Rc weight matrix. **(A3)** Learned Rc weight matrix for CA3 excitatory neurons to CA3 inhibitory neurons. **(A4)** Learned Rc weight matrix for CA3 inhibitory neurons to CA3 excitatory neurons. **(A5)** Learned Sc weight matrix for CA3 excitatory neurons to CA1 neurons. **(B)** Raster plot showing network activity when encoding 10 different inputs (A to J). The activity is depicted for different regions including superficial EC, excitatory neurons in GCL, CA3 excitatory and inhibitory neurons, CA1, and deep EC. We omitted other types of neurons in DG. As in **(A)**, only CA3 excitatory neurons involved in 10 examples of information are selected for visualization. **(C)** CA3 capacity is depicted as the number of engrams formed versus the number of inputs. **(D)** Correlation between input size and CA3 engram size with the linear regression.

suggesting that the DG effectively decorrelates input features through pattern separation before they reach CA3. Figures 5B and 6A illustrate the firing patterns for 10 arbitrary inputs during the encoding and retrieval phases,

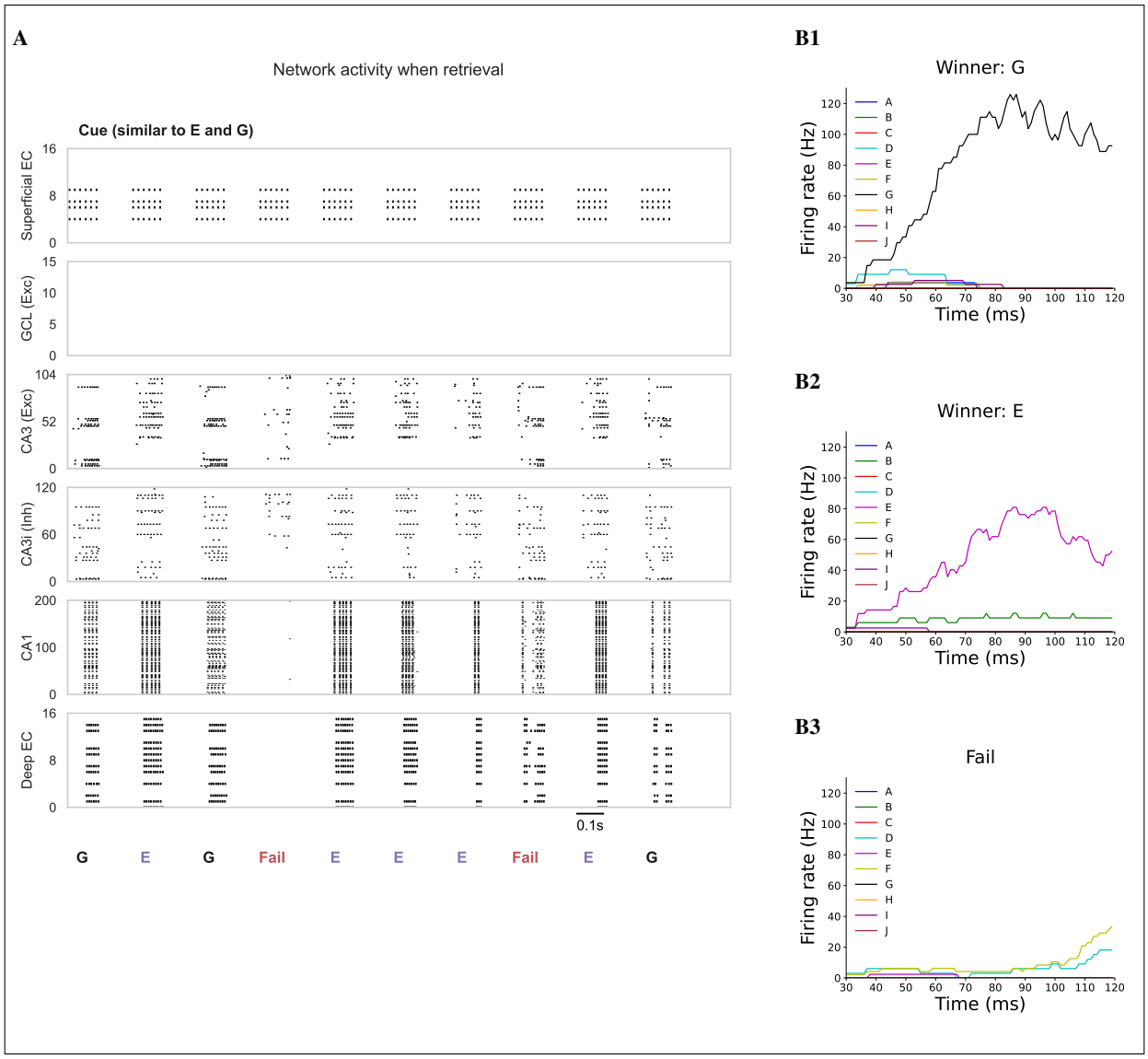

Figure 6: Retrieval for learned inputs. **(A)** Raster plot showing network activity when given a cue similar to E and G for 10 different inputs (A to J). The depicted layers and neurons are the same as Figure 3B. The retrieval cue is repeated 10 times resulting in either successful retrieval (E, G) or retrieval failure as observed by patterns in the deep EC. **(B)** Firing rate over time for neural assemblies during engram competition in CA3, illustrating different scenarios of retrieval competition. **(B1)** Example when G is retrieved, showing a dominant firing rate for engram storing G. **(B2)** Example when E is retrieved, showing a dominant firing rate for engram storing E. **(B3)** Example when retrieval failure where no dominant engram emerges.

respectively. We updated the peak conductances similar to conventional synaptic weights, rather than modifying the synaptic weights directly ('Materials and methods'). This approach keeps the synaptic weights for each connection fixed, thereby maintaining the connectivity ratio. But for readability, we will express the learned weights as the product of the peak conductance and synaptic weights for each connection (Figure 5A).

During encoding, inputs separated by the DG result in distinct firing patterns of excitatory neurons in the GCL which subsequently activate distinct patterns of neurons in CA3, forming sparse distributed patterns Figure 5A2. The learned weights for Rc, connections from excitatory neurons to other excitatory neurons show some weights deviating from the diagonal axis, indicating sparsely distributed storage. In contrast, no diagonal patterns were observed for other types of connections, particularly those involving inhibitory neurons in CA3 (Figures 5A3 and 5A4). This implies that inhibitory neurons are selective to inputs (Figure 2B) but are not specifically constrained to particular engrams.

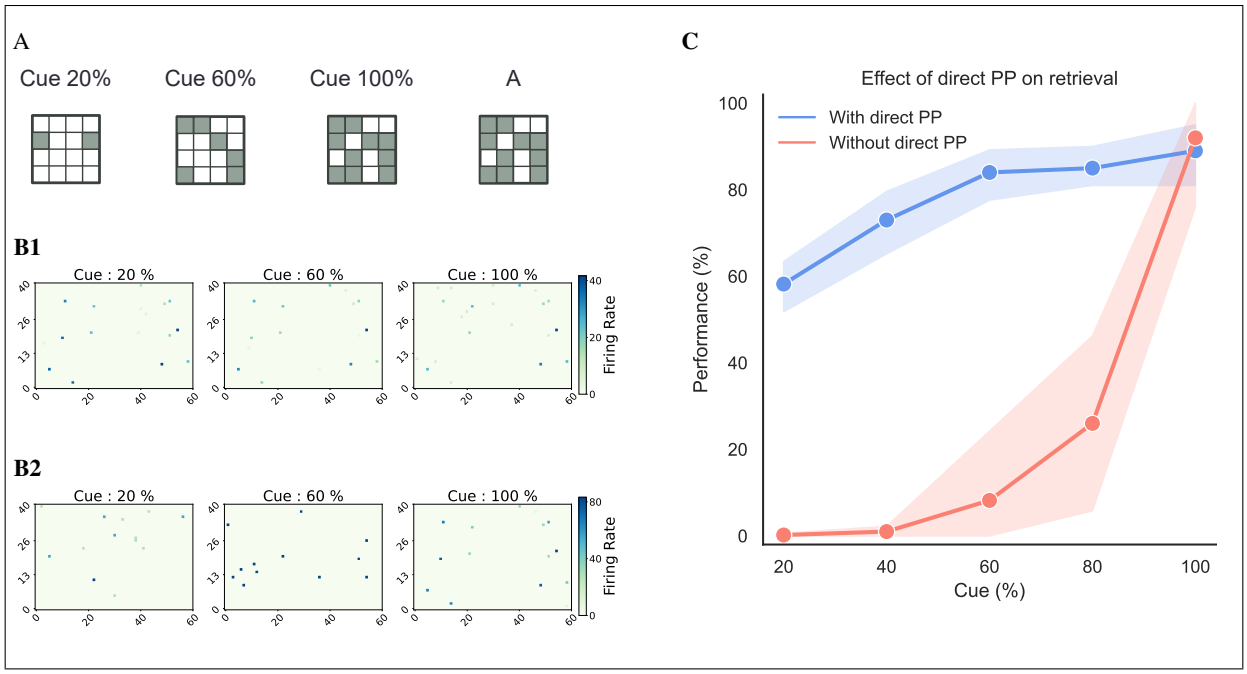

Figure 7: The effect of the direct perforant path for pattern completion during retrieval. **(A)** Illustration of different percentages of partial cues for a learned input A. **(B)** Firing rate heatmap for CA3 neurons when given a cue during retrieval (120ms). Since the model retrieves different outputs for a cue, patterns in the heatmap show the pattern with the highest possibility of retrieval in 20 repetitions. **(B1)** Example of a given cue in the intact direct PP condition. Each heatmap shows similar firing patterns regardless of the cues. **(B2)** Example of a given cue where direct PP is silenced. The heatmaps show different firing patterns for each cue. **(C)** Retrieval performance as a function of percentages of partial cues under two conditions: with direct PP (blue) and without direct PP (red). Performance is measured as the mean success rate for retrieval, averaged over five samples for each percentage of the cue, except for the case of cue 100%, which is based on a single sample. Each sample's success rate is averaged over 20 repetitions.

To observe engram competition during the retrieval phase, we presented an input similar to both E and G (0.5 similarity to each) 10 times during the retrieval phase. The input, sent to the superficial EC, flows to CA3 via the direct PP, acting as a retrieval cue. The noise was introduced to CA3 excitatory neurons at a frequency of 3.5 Hz, representing various factors present in a real brain, which are essential for the attractor network [Webb et al., 2011]. Under these conditions, the model retrieved either input G or E in 80% of the trials. Failures were defined as instances where no clear winner was determined by competition, resulting in interference activation or no activation in the deep EC (Figure 6A). Analysis of the average firing rate with a 30 ms time window for each neural assembly in CA3 showed that only one exhibited a high firing rate during successful pattern completion, indicating that the winning assembly suppresses other assemblies (Figures 6B1 and 6B2). In cases of failed pattern completion, no dominant assembly was observed (Figure 6B3).

These results demonstrate the model's ability to retrieve memories based on their similarity to retrieval cues. Although the DG's output erases specific input features before they reach CA3, the direct PP retains these features. To evaluate the function of direct PP, we deactivated it during retrieval and utilized mossy fibers to send information to CA3. We tested varying percentages of partial cues for each memory to evaluate the role of the direct PP in capturing input completeness (Figure 7A). Figure 7C illustrates retrieval performance, averaged over 5 samples for each percentage of partial cue. The results demonstrate significantly higher success rates when the direct perforant path (PP) is intact, compared to when it is silenced. This is because the DG perceives the cue as distinct information, which activates entirely different neurons in the CA3 region through pattern separation. In contrast, the direct PP stimulates neurons associated with memories similar to the cue (Figures 7B1 and 7B2).

2.5 Stability of pattern completion with selective inhibition under various conditions.

We demonstrated that the model can encode inputs in a sparse and distributed form through pattern separation by the DG, and retrieve these via the direct PP through pattern completion. Additionally, we demonstrated that the model is well-suited for investigating the stability of pattern completion. The sparsely distributed nature of engrams in CA3

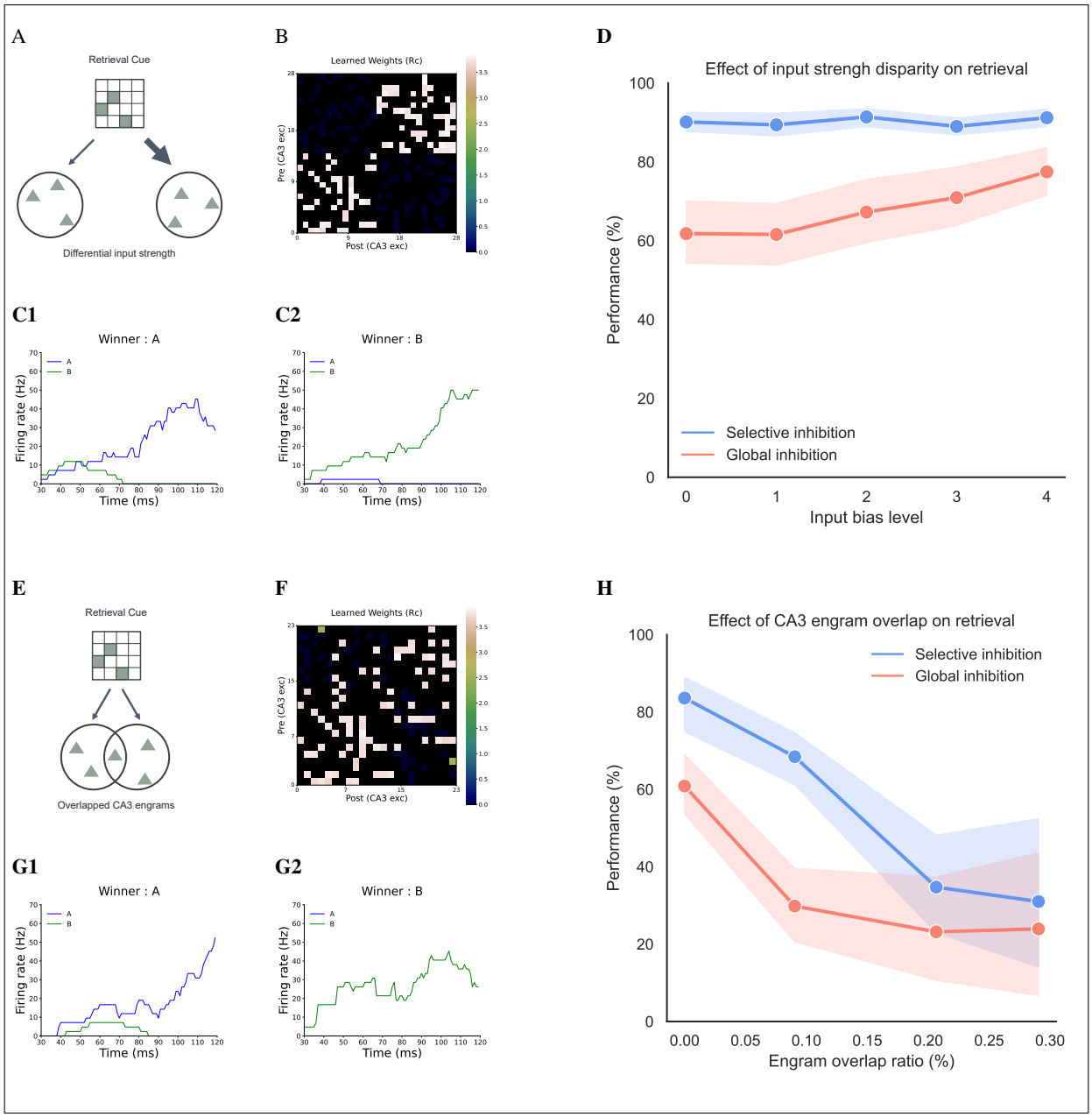

Figure 8: The effect of input strength disparity and overlap ratio between CA3 engrams on retrieval. **(A)** Schematic of the retrieval cue with differential input strengths to each engram. **(B)** Example of the learned weights matrix for Rc in the input strength disparity task. **(C)** Firing rate over time for neural assemblies during engram competition in the input strength disparity task. **(C1)** and **(C2)** are the results for the same cue in the situation where the same samples are learned. **(C1)** Example when A is retrieved. **(C2)** Example when B is retrieved. **(D)** Retrieval performance across different levels of input strength disparity, comparing selective inhibition (blue) and global inhibition (red). Performance is measured as the mean success rate for retrieval, which is an average of over 15 samples for each input bias level. Each sample's success rate is averaged over 50 repetitions. **(E)** Schematic of the retrieval cue with overlapped engrams. **(F)** Example of the learned weights matrix for Rc in the overlap task. **(G)** Firing rate over time for neural assemblies during engram competition in overlap task **(G1)** and **(G2)** are the results for the same cue in the situation where the same samples are learned. **(G1)** Example when A is retrieved. **(G2)** Example when B is retrieved. **(H)** Retrieval performance

Figure 8 continued on next page

Figure 8 continued
across different levels of overlap ratio between neural assemblies, comparing selective inhibition (blue) and global inhibition (red). Performance is measured as the mean success rate for retrieval, which is an average of over 15 samples for each overlap ratio. Each sample's success rate is averaged over 50 repetitions.

can exhibit various properties that may influence engram competition during pattern completion. We identified four key conditions affecting this competition: (1) disparity in input strength to CA3 engrams, (2) overlap between CA3 engrams, (3) number of competing engrams for a single cue, and (4) size differences between CA3 engrams, where size is defined by the number of excitatory neurons involved in each engram. We examined the impact of these conditions on engram competition and compared the retrieval performance of the model under selective inhibition with those under global inhibition alone. To simulate the effects of global inhibition, we maintained constant initial peak conductances from excitatory to inhibitory neurons in CA3. By not applying plasticity to the connections from excitatory neurons to inhibitory neurons in CA3, we removed the capability for selective inhibition.

2.5.1 Robust pattern completion against input strength disparity

According to the encoding specificity principle, retrieval is most effective when the retrieval cue closely matches the features present during the initial encoding of the memory [Tulving and Thomson, 1973, Ji, 2023]. However, retrieval can become challenging due to interference when competing memories share sufficient similarities with the retrieval cue. While this interference can naturally lead to the generalization of competing memories, it becomes problematic when it is necessary to distinguish between these memories. One way to address this challenge is by providing a biased input to one memory, which reduces the similarity of another memory to the cue [Deco and Rolls, 2006]. Nonetheless, when two memories contain highly similar information, introducing a biased input becomes difficult, potentially resulting in poor retrieval performance. This reduces the effectiveness of the dentate gyrus in distinguishing highly similar information. We explored the role of selective inhibition in maintaining the stability of pattern completion, even when cues are uniformly allocated among competing CA3 engrams. We modulated the input bias by adjusting the similarity of cues to one memory relative to another. We varied the number of common neurons shared between the cue and the encoded input (Figure 8A). To isolate the effects of this variable, we selected 15 pairs of inputs, each stored in CA3 engrams of the same size and without overlap between engrams (Figure 8B). Each pair was assigned five different input bias levels, and retrieval was tested 50 times for each level.
Our results showed that when cues were evenly allocated between two CA3 engrams, retrieval performance under global inhibition was approximately 60%. This suggests that non-biased inputs can hinder engram competition, increasing the likelihood of interference between memories, even when those are fully separated (Figure 8D). In contrast, under selective inhibition, retrieval performance remained consistent regardless of disparities in input strength. This consistency is likely because selective inhibition enhances the contrast between competing memories, effectively amplifying small differences in input strength. These findings suggest that selective inhibition can improve the robustness of memory retrieval in the hippocampus by maintaining stable performance even when cues are not biased toward a particular memory.

2.5.2 Pattern completion with overlapping engrams

Next, we examined the impact of overlap between engrams (Figure 8E). In CA3, engrams are encoded using sparse distributed representations, which can lead to varying degrees of overlap. While various mechanisms may exist to mitigate interference caused by overlapping engrams, such overlaps can still interfere with each other, potentially reducing retrieval performance. To investigate this effect, we prepared 60 input pairs, each stored in CA3 engrams of the same size, while varying the overlap ratio (Figure 8F). Each pair of memories received evenly distributed partial cues, and retrieval was tested 50 times.
The results showed that retrieval performance generally declined as the overlap ratio between engrams increased. However, selective inhibition consistently outperformed global inhibition across all overlap ratios (Figure 8H). While selective inhibition was still affected by increasing overlap, it remained more effective than global inhibition. These findings suggest that although selective inhibition's effectiveness decreases with higher overlap, it remains more effective than global inhibition in mitigating interference between overlapping engrams. This shows that selective inhibition aids in maintaining memory integrity, even when engrams are potentially exposed to interference.

2.5.3 Pattern completion performance relative to the number of competing engrams

We also considered scenarios where multiple memories compete for retrieval from a single cue (Figure 9A). As the number of memories associated with a cue increases, it becomes more challenging for the cue to retrieve specific

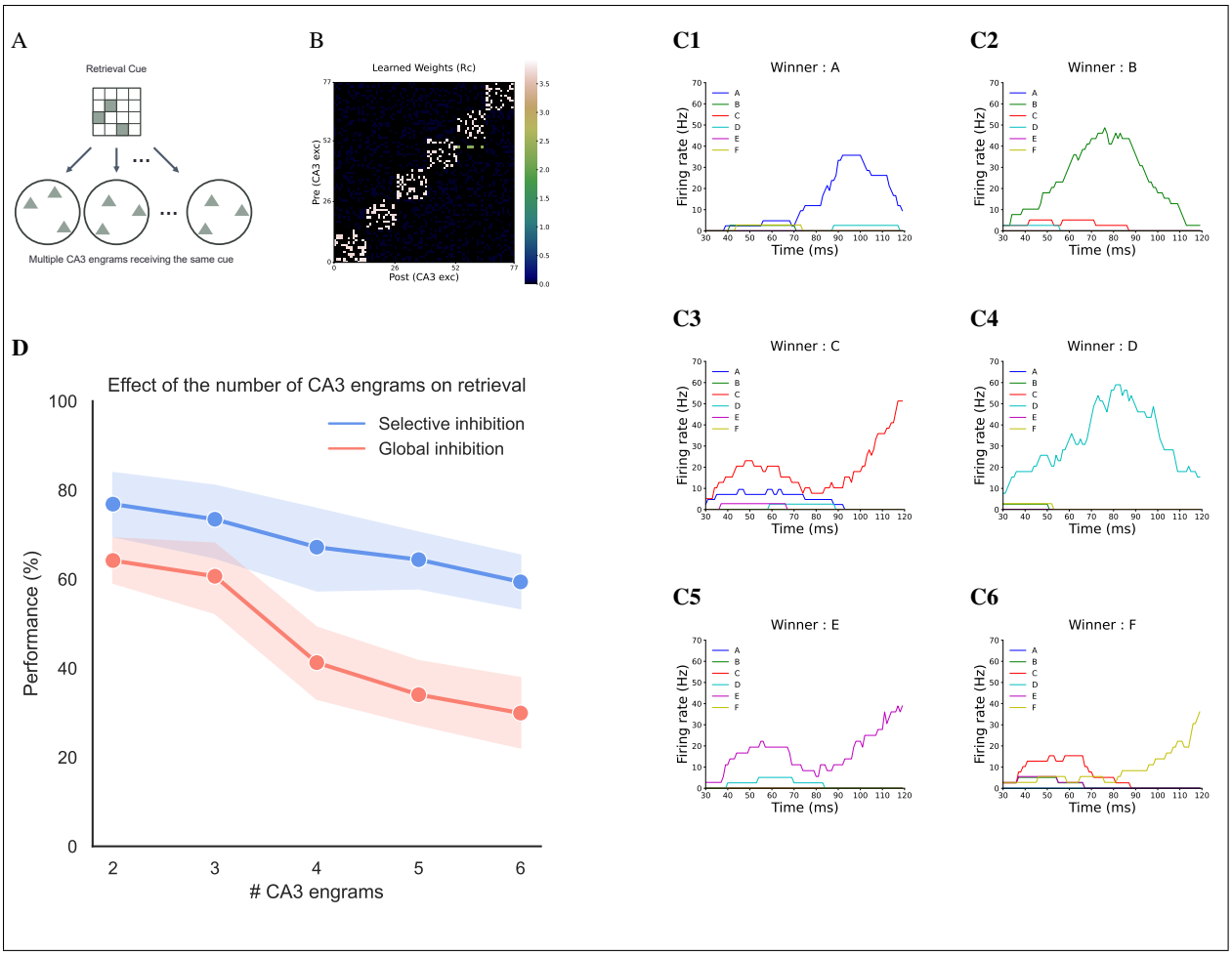

Figure 9: The effect of the number of engrams in CA3 on retrieval. **(A)** Schematic of the retrieval cue with multiple engrams competing for retrieval. **(B)** Example of the learned weights matrix for Rc in the task where multiple engrams compete. **(C)** Firing rate over time for neural assemblies during engram competition **(C1)** to **(C6)** are the results for the same cue in the situation where the same samples are learned. **(C1)** Example when A is retrieved. **(C2)** Example when B is retrieved. **(C3)** Example when C is retrieved. **(C4)** Example when D is retrieved. **(C5)** Example when E is retrieved. **(C6)** Example when F is retrieved. **(D)** Retrieval performance across different numbers of engrams, comparing selective inhibition (blue) and global inhibition (red). Performance is measured as the mean success rate for retrieval, averaged of over 15 samples for each condition involving different numbers of engrams. Each sample's success rate is averaged over 50 repetitions.

memories effectively [Watkins and Watkins, 2013, Parkin, 2007], leading to a natural decrease in retrieval performance. Nonetheless, studying the effects of selective inhibition in this context is worthwhile, as it helps us understand its role in managing situations with multiple competing memories. To explore this, we prepared 75 sets of inputs, each stored in CA3 engrams of the same size and without overlap between engrams, while varying the number of competing engrams (Figure 9B). As in other tasks, each memory received evenly distributed partial cues, and retrieval was tested 50 times. Figure 9D shows that retrieval performance generally decreases as the number of competing engrams increases. While selective inhibition helps maintain relatively higher performance levels, it is not entirely unaffected by the increasing competition. The data suggest that selective inhibition can alleviate some of the negative effects, even as the number of competing memories increases.

2.5.4 Reduced sensitivity to size variations of the engram in CA3 under selective inhibition

In the model, the size of the engram in CA3 shows no correlation with input information (Figure 5), suggesting that size should not inherently affect pattern completion. Ideally, input similarity should have a greater influence than the

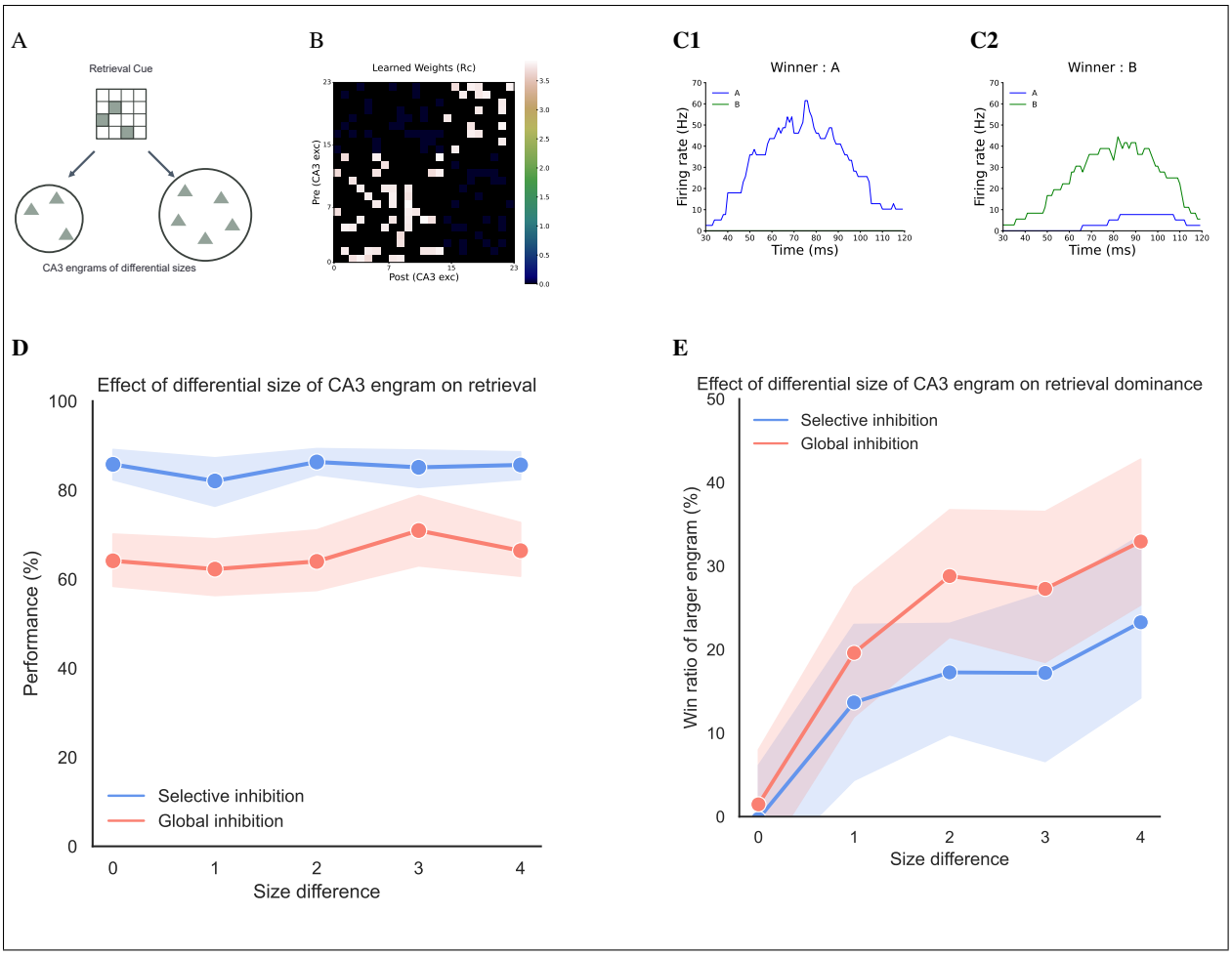

Figure 10: The effect of the size of engrams in CA3 on retrieval. **(A)** Schematic of the retrieval cue with the differential sizes of engrams. **(B)** Example of the learned weights matrix for Rc in the task where engrams have different sizes. **(C)** Firing rate over time for neural assemblies during engram competition. **(C1)** and **(C2)** are the results for the same cue in the situation where the same samples are learned. **(C1)** Example when A is retrieved. **(C2)** Example when B is retrieved. **(D)** Retrieval performance across the size difference between engrams, comparing selective inhibition (blue) and global inhibition (red). Performance is measured as the mean success rate for retrieval, which is an average of over 15 samples for each size difference. Each sample's success rate is averaged over 50 repetitions. **(E)** Retrieval dominance of memory stored in larger engrams across the size difference between them, comparing selective inhibition (blue) and global inhibition (red). Retrieval dominance indicates the percentage of times the memory with the larger engrams is retrieved.

engram size to avoid scenarios where a less similar memory is easier to retrieve merely due to the larger size of its engram. We investigated the impact of the size differences to determine whether the larger engram has an advantage in retrieval and how selective inhibition manages this size disparity compared to global inhibition (Figure 10A). We prepared 75 sets of input pairs, each stored in CA3 engrams with varying engram sizes and with no overlap between the engrams (Figure 10B). Each memory received partial cues evenly, and retrieval was tested 50 times.

The results show consistent retrieval performance, with the condition involving selective inhibition generally outperforming global inhibition due to the evenly distributed cue strength (Figure 10D). However, the engram size influenced which memory was retrieved; memories stored in larger engrams were more likely to dominate the retrieval process, particularly under conditions of global inhibition (Figure 10E). The competition in this scenario revealed a tendency for memories stored in larger engrams to be retrieved more frequently, highlighting the potential limitations of global inhibition in managing engram competition.

Our findings demonstrate that selective inhibition provides a robust mechanism for pattern completion across various conditions affecting engram competition. It enhances retrieval performance regardless of input strength disparity,

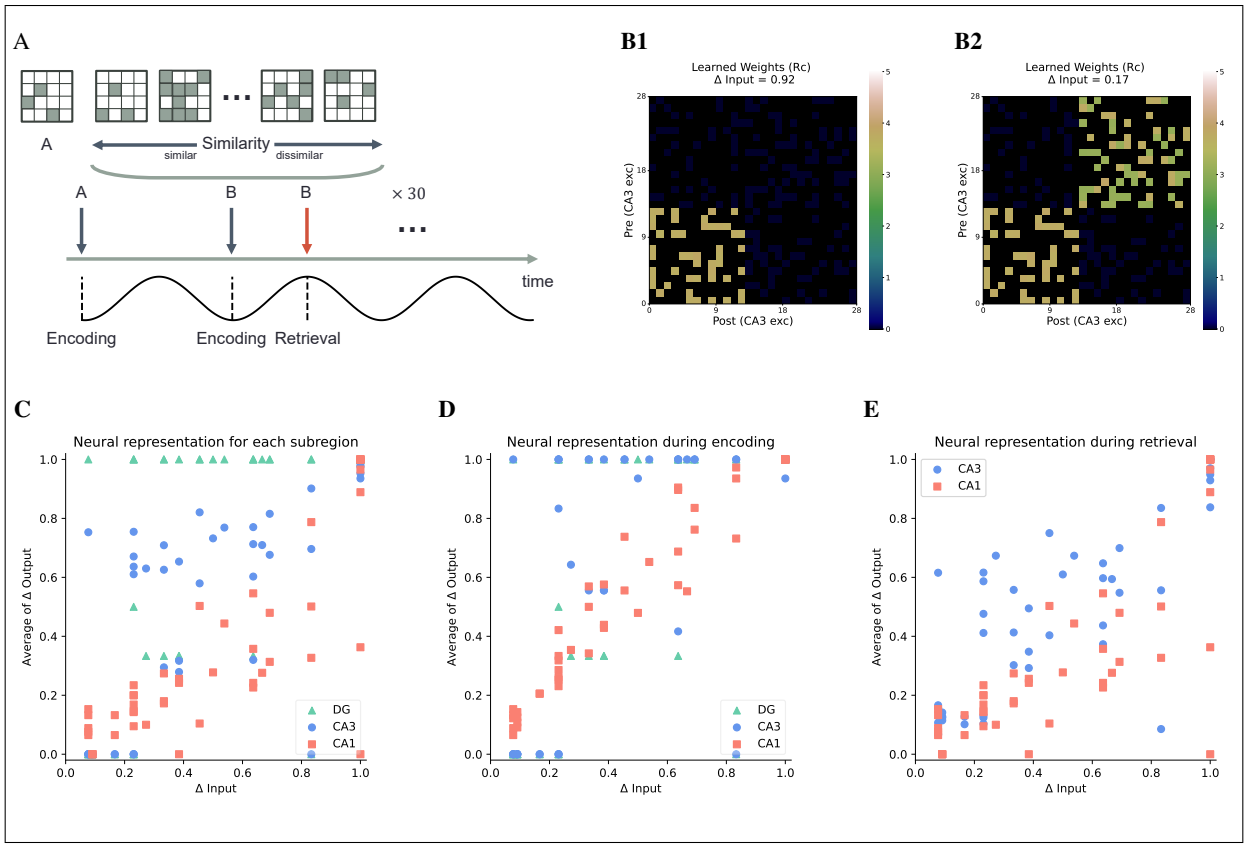

Figure 11: **(A)** Schematic of the pattern separation task. Input A is presented to the model during a single encoding phase (120 ms) while input B is presented over 7.2 seconds (30 phases), with both encoding and retrieval phases. Input B is varied in similarity to Input A across 105 trials to assess the model's ability to perform pattern separation. **(B)** Examples of the learned weights matrices for Rc in CA3 for **(B1)** highly similar (Δ Input $= 0.92$) and **(B2)** less similar (Δ Input $= 0.17$) input patterns. **(C)** Changes in Neural representations for each subregion in the model over the input discrimination (Δ Input). Input discrimination is divided into 20 windows. For each window, the Δ outputs are averaged over 30 phases, and these averaged outputs are further averaged for each window. **(D)** Neural representation changes for each subregion in the model over the input discrimination (Δ Input) during the encoding phase. **(E)** Neural representation changes for each subregion in the model over the input discrimination (Δ Input) during the retrieval phase.

mitigates the negative effects of overlap between engrams, maintains higher performance levels as the number of competing memories increases, and effectively manages size differences between engrams. These results underscore the advantages of selective inhibition over global inhibition in ensuring reliable memory retrieval and suggest its potential role in the hippocampus for managing complex memory dynamics.

2.6 Neuronal representations across hippocampal subregions during pattern separation and pattern completion task.

We expanded our investigation to focus on pattern separation across the entire hippocampal model, building on our observations of stable pattern completion under various conditions facilitated by selective inhibition. Previous studies have shown that different hippocampal subregions exhibit distinct patterns of neuronal activation [Yassa and Stark, 2011, Knierim and Neunuebel, 2016]. We conducted 105 trials, varying the similarity between inputs A and B to explore this (Figures 11A and 11B). Input A was presented during a single encoding phase (120 ms), while input B was presented over 7.2 seconds across 30 phases, covering both encoding and retrieval (Figure 11A).
To quantify the discrimination between neuronal patterns A and B, we averaged the discrimination values across 30 phases. Our analysis revealed distinct computational characteristics for each hippocampal subregion. The DG exhibited robust pattern separation capabilities, demonstrating effective separation between input patterns, especially when the input dissimilarity Δ input exceeded 0.2. In contrast, CA1 exhibited a linear relationship between input and output

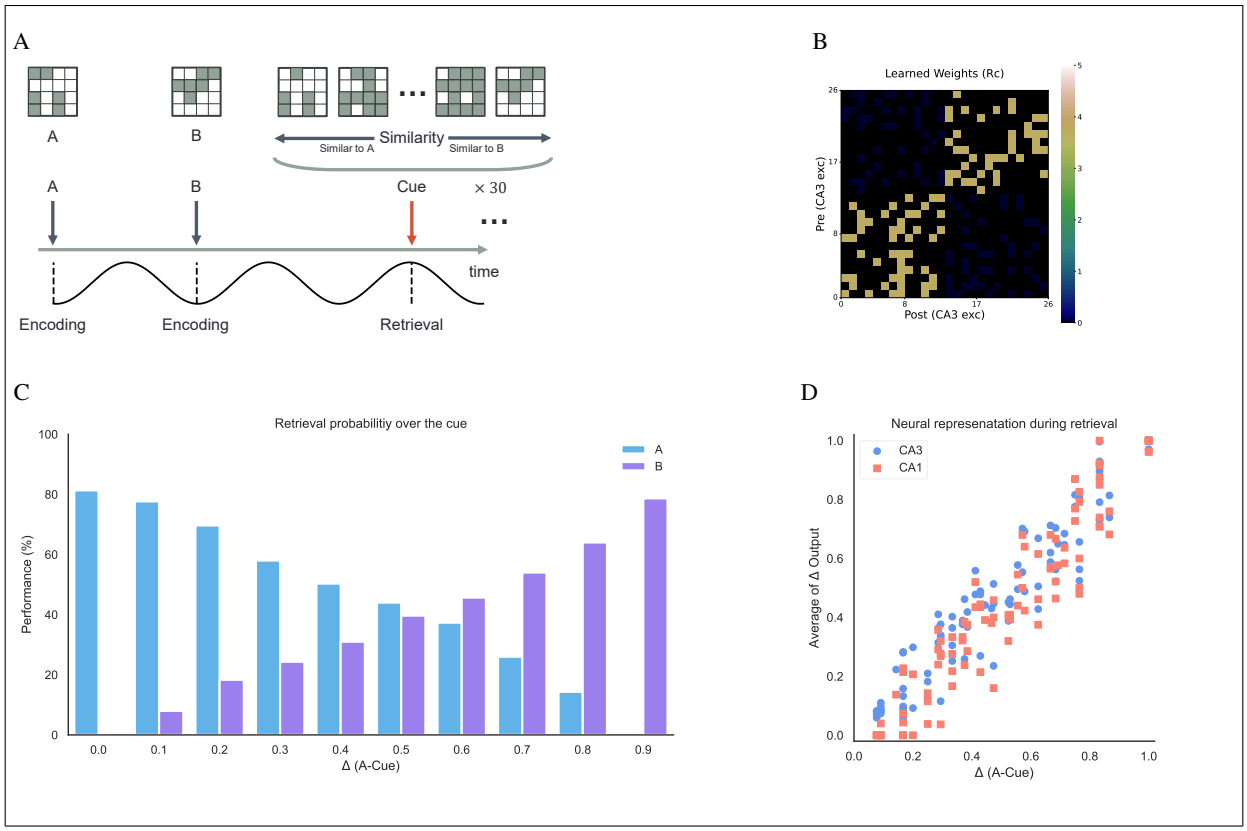

Figure 12: **(A)** Schematic of the pattern completion task. Both inputs A and B are presented to the model during an encoding phase (120 ms). The similarity between inputs A and B is set to 0. During the retrieval phase, the 100 cues are given with a linearly proportionally relationship between their similarity to A and B, maintaining the sum of the similarities to A and B as 1. Each cue is presented for 7.2 seconds and we observed 30 retrieval phases without further learning. **(B)** The learned weight matrix for Rc after training with inputs A and B. **(C)** Retrieval performance over the similarity between input A and Cue (Δ A$-$Cue). The performance is measured as the probability of retrieving Input A (blue) or Input B (purple) in response to the presented cue with 30 retrieval phases. **(D)** Neural representation changes over the discrimination between input A and cues (Δ A$-$Cue) during the retrieval. Input discrimination is divided into 20 windows. For each window, the Δ outputs are averaged over 30 phases, and these averaged outputs are further averaged for each window.

discrimination, indicating a more gradual differentiation process (Figure 11C). This finding is consistent with evidence suggesting that the DG possesses a unique capability to discriminate between similar inputs [Neunuebel and Knierim, 2014, Berron et al., 2016]. In the CA3 region, Δ output tended to be lower than CA1 when the Δ input was below 0.2. This indicates that CA3 experiences reduced efficiency in pattern separation for highly similar inputs. However, as Δ input increased beyond 0.2, CA3's Δ output surpassed that of CA1, indicating enhanced separation capabilities for more distinct inputs (Figure 11C). These results are consistent with previous studies [Lee et al., 2004, Leutgeb et al., 2004, Guzowski et al., 2004], though the predicted sigmoidal curve for CA3 was less pronounced in the model [Yassa and Stark, 2011, Knierim and Neunuebel, 2016].

We investigated these Δ output patterns by separating the encoding and retrieval phases to understand the reasons for these behaviors. During encoding, CA3 closely mirrored the pattern observed in the DG, while CA1 displayed a more linear response (Figure 11D). This similarity is due to CA3 receiving information from DG during the encoding phase in the model. At low levels of Δ input, the lower output discrimination in CA3 is attributed to a failure of pattern separation in the DG, indicating that the model perceived two distinct inputs as identical. This observation elucidates the lower output discrimination exhibited by CA3 compared to CA1, as shown in Figure 11C.

During retrieval, the pattern of CA3 more closely resembled that of CA1, consistent with the model's design where CA3 transmits information to CA1 (Figure 11E). Notably, Δ output of CA3 during retrieval was lower than during encoding, despite the intact input B being provided as the cue. This resulted in CA3 appearing to have lower pattern separation performance than DG in Figure 11C, even though CA3 retains the outcomes of DG's pattern separation

during encoding (Figure 11D). This effect was observed even at high Δ outputs (around 0.8), where input B did not consistently converge to its own representation due to the competing influence of pattern completion involving input A (Figure 11E).
To gain deeper insights into the dynamics of pattern completion, we designed a pattern completion task. We examined how varying degrees of similarity between retrieval cues and stored memories affect retrieval accuracy. Specifically, we used an input pair with zero similarity (A and B) as stored memories. During retrieval, we introduced cues with graded similarities to inputs A and B, maintaining a linear proportional relationship between each cue's similarity to A and B (Figure 12A). For example, if a cue was 0.7 similar to A, it would be 0.3 similar to B. This linear progression allows for a more precise analysis of the transition between retrieving different memories compared to arbitrary cue selection.
The results demonstrated a robust linear relationship between cue similarity and retrieval accuracy, indicating that the hippocampal model's pattern completion mechanism is proportionately influenced by the degree of similarity between the retrieval cue and the stored memory (Figure 12D). This linear relationship indicates that even minimally similar cues can contribute to accurate memory retrieval, highlighting the model's sensitivity and precision in pattern completion (Figure 12C). These findings provide valuable insights into the specific mechanisms of pattern completion within our hippocampal model, enhancing our understanding of memory processes.

3 Discussion

We developed a spiking neural network model based on theta oscillation theory that captures the structural and connectivity properties of the hippocampus. In our exploration of memory processing through the model, we focused on the contributions of inhibitory neurons in CA3. Our findings suggest that activation of these neurons during encoding can lead to selective inhibition during retrieval. That is, the role of inhibitory neurons includes selective inhibition in addition to sparse distributed coding in CA3. In the proposed model, inhibitory neurons associated with specific neural assemblies in CA3 selectively suppress excitatory neurons involved in other competing assemblies.
Interestingly, inhibitory neurons do not suppress excitatory neurons within the same engram. This occurs because only excitatory neurons that are not suppressed by inhibitory neurons survive to form neural assemblies. These roles of inhibitory neurons in memory processing within the model are supported by experimental evidence, including (1) feedforward inhibition of the dentate gyrus via mossy fibers, (2) plasticity in inhibitory neurons, (3) heterosynaptic plasticity across the hippocampus, and (4) the segregation of encoding and retrieval phases by theta oscillation.

3.1 Model validation for memory formation

During encoding in the model, inhibitory neurons in CA3 receive inputs via mossy fibers from the DG. These neurons subsequently suppress most excitatory neurons in CA3, determining which neurons remain active. Some observations from the literature, although not all fully specific to the hippocampus, align with the proposed model: Granule cells in the DG are known to recruit feedforward inhibition via mossy fibers [Ruediger et al., 2011, Guo et al., 2018, Viana da Silva et al., 2019]. Parvalbumin-positive (PV+) inhibitory neurons in the hippocampus play a crucial role in memory storage [Korotkova et al., 2010, He et al., 2021, Raven and Aton, 2021]. Inhibitory neurons influence the size of the engram [Morrison et al., 2016, Stefanelli et al., 2016, Josselyn and Tonegawa, 2020, Giorgi and Marinelli, 2021]. These experimental findings highlight the importance of inhibitory neurons in memory formation, indicating that the model effectively captures their functional and structural properties.
Inhibitory neurons in the model have stimulus-selectivity because the DG processes and separates external inputs before transmitting them to CA3. This feature parallels the stimulus-selectivity primarily observed in inhibitory interneurons in the visual and auditory cortices [Li et al., 2014, Khan et al., 2018, Cummings et al., 2021], implying that similar mechanisms may exist in the hippocampus. In this context, inhibitory neurons in sensory areas play a more active role in information processing than previously thought. In line with these findings, the model supports the view that inhibitory neurons in the hippocampus may actively participate in both encoding and retrieval processes while exhibiting stimulus selectivity."
Observations of plasticity in inhibitory neurons indicates their synaptic interactions with excitatory neurons [Pelletier and Lacaille, 2008, Korotkova et al., 2010, Perez et al., 2001, Owen et al., 2013, Cohen et al., 2016, He et al., 2021]. In the model, this plasticity enables inhibitory neurons to modulate their synaptic strengths with excitatory neurons, facilitating selective inhibition during engram competition. Selective inhibition positions inhibitory neurons as active participants in retrieval processes, highlighting their potential contribution to pattern completion.
To effectively harness the properties of inhibitory neurons mentioned above, the model employs two key mechanisms: theta oscillation theory [Hasselmo and Stern, 2014, Kragel et al., 2020, Reddy et al., 2021, Ter Wal et al., 2021, Lowet et al., 2023, Gattas et al., 2023] and heterosynaptic plasticity [Tsukamoto et al., 2003, Hunt et al., 2013, Chater and Goda, 2021, Jenks et al., 2021]. Theta oscillation theory posits that distinct phases of the theta rhythm modulate different information flows in the hippocampus, where encoding takes place at the trough and retrieval at the peak. The

hippocampus maintains distinct phases through phasic changes in membrane potential [Hasselmo and Stern, 2014, Malezieux et al., 2020].
In the model, reflecting these phenomena, synaptic activity associated with retrieval is suppressed during encoding. During the formation of engrams in CA3, heterosynaptic plasticity ensures that connections between inhibitory and excitatory neurons are strengthened, even without direct stimulation. These mechanisms, in particular, enable inhibitory neurons to play an active role, facilitating both sparse distributed coding for pattern separation and selective inhibition for pattern completion.
Proposed model illustrates the rapid process of hippocampal memory formation, completed in just 120 milliseconds. This rapid storage capability reinforces the model's functional plausibility by effectively replicating the rapid memory formation observed in the hippocampus [Moser and Moser, 2003, Lee et al., 2015, Liao and Losonczy, 2024]. Moreover, the model's robust pattern completion across various competitive scenarios supports its functional relevance. This stability indicates that the model effectively captures key aspects of how the hippocampus retrieves memories across different engram configurations.

3.2 Alignment with cognitive evidence

The enhanced stability of the model, driven by selective inhibition, allowed us to investigate firing patterns across hippocampal subregions during pattern separation and completion, by quantitatively controlling similarity. The different functions of subregions during pattern separation and completion are well-documented in the literature [Yassa and Stark, 2011, Knierim and Neunuebel, 2016]. The DG is notably robust in supporting pattern separation [Leutgeb et al., 2007, Santoro, 2013, Neunuebel and Knierim, 2014, Berron et al., 2016]. In CA1, output discrimination is considered linearly related to input discrimination, implying that output differences increase at a constant rate with input differences [Guzowski et al., 2004, Yassa and Stark, 2011, Knierim and Neunuebel, 2016]. CA3, however, exhibits more complex dynamics, since it participates in both pattern separation and pattern completion. Some studies suggest that CA3 is more involved in pattern separation, while others propose a greater role in pattern completion [Leutgeb et al., 2004, Lee et al., 2004, Guzowski et al., 2004].
The model successfully replicates the distinct roles of subregions in these processes, showing strong pattern separation performance in the DG and a consistent linear response in CA1. For CA3, the proposed model aligns with the evidence above across the entire phase. It displays either pattern separation or pattern completion depending on the discrimination of input pairs. We effectively investigated CA3's behavior by separating the encoding and retrieval phases. When the difference between inputs is small, the difference of output pairs in CA3 is reduced compared to that in CA1. This occurs because the pattern separation in the DG does not reach the discrimination threshold during encoding. As a result, the model interprets the two similar inputs as identical and performs pattern completion.
When the difference is large, CA3 shows less pattern separation than the DG, though still more than CA1. The reduced separation is likely due to mixed outcomes, where two completely different memories are retrieved. In other words, there remains a possibility that the cue may still trigger pattern completion for less similar memories, even when it is highly similar to a specific memory. This is supported by the fact that the retrieval probability depends linearly on the similarity between the cue and the memory. Such linearity prevents the dominance of biased memories in retrieval, partially capturing the complexity of real-world information. Since the proposed model aligns with established cognitive data, it may serve as a valuable tool for understanding hippocampal functions. The investigation for phase-specific dynamics offers new insights into how the hippocampus handles conflicting information.

3.3 Limitations and future works

Our current model has several limitations that should be considered in future research. One of the key features of the proposed model is that heterosynaptic plasticity in the connections from excitatory to inhibitory neurons in CA3 elicits selective inhibition. However, there is not yet sufficient evidence to support the presence of heterosynaptic plasticity at these connections.
By simplifying the DG to focus solely on spatial pattern separation with a fixed frequency of input activation, we overlook its well-known roles in temporal and rate pattern separation [Pernía-Andrade and Jonas, 2014, Madar et al., 2019, Löffler and Gupta, 2022]. Due to this simplification, certain details do not fully align with biological specifics, such as the number of neurons in each subregion, the connection probabilities between subregions, and the synaptic weights. Given that these differences may impact the memory retrieval process, the observed linear relationship between similarity and retrieval probability in the pattern completion task should be interpreted with caution, necessitating further experimental validation and larger-scale modeling.
We limited CA1's role to the reinstatement of original information from CA3 engrams, which overlooks the neuronal diversity and complex functions of CA1 [Masurkar, 2018, Jeong and Singer, 2022]. The model disregards cellular-level processes, feedback connections, and molecular signaling pathways (e.g., cAMP Response Element-Binding Protein (CREB)-mediated) [Pelletier and Lacaille, 2008, Josselyn and Tonegawa, 2020, Bickle, 2021]. Since these elements are

acknowledged as key components of memory processes, their omission could constrain the quantitative accuracy of the model's outcomes.
In future work, we will extend the model to incorporate sequential learning, exploring how inhibitory neurons contribute to engram formation and their competition across sequences of information. This extension could enhance our understanding of hippocampal function in processing sequences, leading to deeper insights into cognitive processes such as replay, sequence compression, and predictive coding.

3.4 Conclusion

Our research highlights the active and dynamic role of inhibitory neurons in CA3 engram formation and stable pattern completion. This work offers a fresh perspective on established hippocampal functions and opens new avenues for experimental investigation. As our understanding of hippocampal circuitry and function evolves, models like ours will be crucial in bridging the gap between cellular mechanisms and cognitive phenomena. This approach will advance research in both neuroscience and artificial intelligence.

4 Methods and Materials

4.1 Model structure

To investigate memory formation and competition dynamics, we constructed a spiking neural network model of the hippocampal trisynaptic circuit (superficial EC to CA1 via DG and CA3). The model preserves key pathways, including the mossy fiber projections from DG and the direct perforant path (PP) from superficial EC. We focused solely on spatial pattern processing, excluding temporal sequences for simplicity. The model's input layer consists of 16 neurons, each firing at a fixed rate of 50 Hz. This configuration allows for 2^{16} unique spatial patterns, providing sufficient variability to assess the model's performance while maintaining computational feasibility.
Given our focus on spatial patterns, we only considered spatial pattern separation in DG, omitting temporal and rate separation mechanisms. This simplification necessarily leads to deviations from biological details regarding the number of neurons in each subregion, connection probabilities between subregions, and synaptic weights (Tables 2 and 3). The parameters were derived from the study Chen [2017] and were optimized with significant modifications through iterative manual adjustments to ensure the model's proper functioning. We initialized and fixed connection weights with specific values for each connection during learning to maintain connection probabilities. Instead of adjusting these connection weights, we modified the peak conductance analogous to conventional connection weights. These were initialized to 0, except for connections from inhibitory neurons to excitatory neurons in CA3, to establish global inhibition as the default state (detailed explanation in the next section).
The CA1 region in our model is simplified, consisting only of excitatory neurons. Although this simplification omits some of the intricate microcircuitry present in biological CA1 [Masurkar, 2018, Jeong and Singer, 2022], it retains the essential function of interfacing between CA3 and EC, facilitating the reinstatement of original information by CA3 engrams. We artificially designed the CA1-EC connections so that each CA1 neuron maintains consistent bidirectional connections with specific EC neurons. This arrangement, while not strictly biological, allows CA3 engrams to efficiently encode and decode information between hippocampal and cortical representations.
We implemented our model using Python with NumPy. The following sections detail the specific neuron models, learning rules, and analysis methods used to investigate memory dynamics within this structure.

4.2 Single neuron models

Each neuron was described using the Izhikevich model [Izhikevich and Edelman, 2008] following as

$$C\dot{v} = k(v - v_r)(v - v_t) - u - I_{syn} \tag{1}$$

$$\dot{u} = a\{b(v - v_r) - u\} \text{ if } v \geq 30mV, \text{ then } v = c, u = u + d \tag{2}$$

Table 1: Parameters of Izhikevich model for excitatory neurons and inhibitory neurons.

	C	k	V_{rest}	V_{th}	V_{peak}	a	d	c	d
Exc	80	3	-60	-50	50	0.01	5	-60	10
Inh	20	1	-55	-40	25	0.15	8	-55	200

where C is the membrane capacitance, v is the membrane potential, v_r is the resting potential, v_t is the threshold potential, and u is the recovery variable (the difference of all inward and outward voltage-gated currents) [Izhikevich and Edelman, 2008]. I_{syn} is the summation of synaptic currents from other neurons, detailed in the next section. Each parameter, including the dimensionless values k, a, b, c, and d, follows the values specified by Izhikevich and Edelman [2008] for different neuron types. Based on this paper, the excitatory neurons use the parameters for pyramidal cells, and the inhibitory neurons use those for basket interneurons (Table 1).

4.3 Synapse models

The total synaptic current model also follows [Izhikevich and Edelman, 2008, Chen, 2017], which consists of four basic conductances from AMPA, NMDA, $GABA_A$, and $GABA_B$ channels with the simplified voltage-gating of the NMDA channel ($[(v+80)/60]^2/[1+((v+80)/60)^2]$).

$$I_{syn} = g_{AMPA}(v-0) + g_{NMDA}\frac{\left[(v+80)/60\right]^2}{1+\left[(v+80)/60\right]^2}(v-0) + g_{GABA_A}(v+70) + g_{GABA_B}(v+90) \tag{3}$$

$$\begin{cases} g = g + q & \text{if } v \geq 30mV \\ \dfrac{dg(t)}{dt} = -\dfrac{1}{\tau}g(t) & \text{otherwise} \end{cases} \tag{4}$$

where the reversal potentials of AMPA and NMDA channels are 0 mV and reversal potentials for $GABA_A$ and $GABA_B$ channels are -70 mV and -90 mV respectively. The ratio of NMDA to AMPA receptors was set to 5:5, and the ratio of $GABA_A$ to $GABA_B$ receptors was set to 9:1 for all of the neurons in CA3 [Chen et al., 2013]. For simplification, the synapse models of neurons in the DG included only AMPA and $GABA_A$ receptors because learning does not occur in this region of the model (Table 2).
Synaptic conductance decreases exponentially with different time constants and increases by the peak conductance q upon the arrival of an action potential at the synapse [Chen and Wang, 2007]. The total excitatory and inhibitory synaptic currents were limited to maximum values of W_{Be} and W_{Bi} respectively (Table 2). For excitatory neurons in CA3, the total synaptic current was differentiated based on the region of origin of the sending neuron—superficial EC, DG, or CA3—to preserve the distinct influences of each region. Additionally, some connections featured delayed transmission times to the postsynaptic neuron to ensure stable learning (Table 3).

4.4 STDP learning

Learning was implemented using symmetric STDP [Mishra et al., 2016, Ecker et al., 2022]. Instead of directly adjusting the synaptic weights W, we updated the peak conductance q to maintain the connectivity ratio within the network. Synaptic weights, which are typically involved in scaling the current, were initialized and held constant throughout the learning process to preserve the network's initial structure and stability [Chen and Wang, 2007]. This approach

Table 2: Parameters for neurons organizing each layer.

	N	τ_{AMPA}	τ_{NMDA}	τ_{GABA_A}	τ_{GABA_B}	W_{Be}	W_{Bi}
superficial EC	16	5	-	-	-	5	-
deep EC	16	5	-	-	-	5	-
Hilus(Exc)	100	5	-	15	-	5	10
Hilus(Inh)	16	5	-	-	-	5	-
GCL(Exc)	800	5	-	15	-	5	10
GCL(Inh)	400	5	-	-	-	7	7
CA3(Exc)	2400	5	30	8	30	4, 0.75, 20	10
CA3(Inh)	120	5	30	8	30	5	10
CA1	200	5	30	-	-	4	-

ensures that the modifications introduced by STDP do not disrupt the overall connectivity but instead refine the existing connections. (Table 3).

$$q = q + F(\Delta t),\ F(\Delta t) = \begin{cases} A_+ \exp\left(-\dfrac{\Delta t}{\tau_+}\right) & \text{at } t_{post},\ \text{if } t_{pre} < t_{post} \\ A_- \exp\left(\dfrac{\Delta t}{\tau_-}\right) & \text{at } t_{pre},\ \text{if } t_{post} < t_{pre} \end{cases} \tag{5}$$

where $\Delta t = t_{post} - t_{pre}$ represents the time difference between action potentials, and $A_\pm$ determines the maximum amount of synaptic modification, which decays exponentially with time constants $\tau_\pm$. The peak conductance is constrained within the range [0, q_{max}], where $q_{max} = 3$ nS. Given the symmetric nature of the STDP rule adopted, $A_\pm$ was set to 0.2 nS, and $\tau_\pm$ was set to 62.5 ms.

4.5 Similarity analysis

Our model focuses exclusively on spatial input patterns and spatial pattern separation. Therefore, the similarity between firing patterns was assessed by calculating the spatial overlap, as suggested by Löffler and Gupta [2022].

$$O_{ij} = \frac{n_i}{n_i + n_j} \tag{6}$$

where n_i represents the number of activated neurons in pattern i, and n_{ij} denotes the number of neurons activated in both patterns i and j. The discrimination value Δ between patterns i and j is calculated as $1 - O_{ij}$. The firing pattern is determined based on neuron activation, except for the case of CA3. For CA3 patterns during retrieval, only neurons firing at rates exceeding 25 Hz are considered, ensuring that only significant activity is captured and noise is effectively filtered out. This threshold helps to isolate meaningful firing patterns that contribute to memory retrieval, thereby enhancing the accuracy of the pattern analysis.

Table 3: Parameters for connections between layers.

	p_{conn}	W	t_d
Superficial EC→Hilus (Exc)	0.3125	3	-
Superficial EC→Hilus (Inh)	One-to-One	3	-
Superficial EC→GCL (Exc)	0.0625	2	10
Superficial EC→GCL (Inh)	0.5	4	-
Superficial EC→CA3 (Exc)	0.25	2	-
Superficial EC→Deep EC	One-to-One	3	-
Deep EC→CA1	0.125	0.75	-
Hilus (Inh)→Hilus (Exc)	0.0625	4	-
Hilus (Exc)→GCL (Inh)	0.5	4	-
GCL (Inh)→GCL (Exc)	0.0013	3	-
GCL (Exc)→CA3 (Exc)	0.0125	2	3
GCL (Exc)→CA3 (Inh)	0.025	2	-
CA3 (Exc)→CA3 (Exc)	0.25	1	5
CA3 (Exc)→CA3 (Inh)	0.25	1	-
CA3 (Exc)→CA1	0.5	0.45	-
CA3 (Inh)→CA3 (Exc)	0.25	5	-
CA1→Deep EC	0.125	2	15

References

J. O'Keefe and L. Nadel. *The hippocampus as a cognitive map*. Clarendon Press, Oxford, United Kingdom, 1978.

Endel Tulving. *Elements of Episodic Memory*. Oxford University Press, 1983.

Richard Wolfgang Semon, Betty Duffy, and Vernon Lee. *Revival: Mnemic Psychology (1923)*. Routledge, 1st edition, 1923. doi:10.4324/9781351253529.

Sheena A. Josselyn and Susumu Tonegawa. Memory engrams: Recalling the past and imagining the future. *Science*, 367(6473):eaaw4325, 2020. doi:10.1126/science.aaw4325.

John T. Wixted, Larry R. Squire, Yoonhee Jang, Megan H. Papesh, Stephen D. Goldinger, Joel R. Kuhn, Kris A. Smith, David M. Treiman, and Peter N. Steinmetz. Sparse and distributed coding of episodic memory in neurons of the human hippocampus. *Proceedings of the National Academy of Sciences*, 111(26):9621–9626, 2014. doi:10.1073/pnas.1408365111.

David Marr. Simple memory: a theory for archicortex. *Philosophical Transactions of the Royal Society of London. B, Biological Sciences*, 262:23–81, 1971. doi:10.1098/rstb.1971.0078.

James L. McClelland, Bruce L. McNaughton, and Randall C. O'Reilly. Why there are complementary learning systems in the hippocampus and neocortex: insights from the successes and failures of connectionist models of learning and memory. *Psychological Review*, 102(3):419–457, 1995. doi:10.1037/0033-295X.102.3.419.

David Berron, Hartmut Schütze, Anne Maass, Arturo Cardenas-Blanco, Hugo J. Kuijf, Dharshan Kumaran, and Emrah Düzel. Strong evidence for pattern separation in human dentate gyrus. *Journal of Neuroscience*, 36(29):7569–7579, 2016. ISSN 0270-6474. doi:10.1523/JNEUROSCI.0518-16.2016.

Edmund T. Rolls. Pattern separation, completion, and categorisation in the hippocampus and neocortex. *Neurobiology of Learning and Memory*, 129:4–28, 2016. ISSN 1074-7427. doi:https://doi.org/10.1016/j.nlm.2015.07.008.

James J. Knierim and Joshua P. Neunuebel. Tracking the flow of hippocampal computation: Pattern separation, pattern completion, and attractor dynamics. *Neurobiology of Learning and Memory*, 129:38–49, 2016. ISSN 1074-7427. doi:https://doi.org/10.1016/j.nlm.2015.10.008.

Jill K. Leutgeb, Stefan Leutgeb, May-Britt Moser, and Edvard I. Moser. Pattern separation in the dentate gyrus and ca3 of the hippocampus. *Science*, 315(5814):961–966, 2007. doi:10.1126/science.1135801.

A. Treves, A. Tashiro, M.P. Witter, and E.I. Moser. What is the mammalian dentate gyrus good for? *Neuroscience*, 154 (4):1155–1172, 2008. ISSN 0306-4522. doi:https://doi.org/10.1016/j.neuroscience.2008.04.073.

Michael A Yassa and Craig E L Stark. Pattern separation in the hippocampus. *Trends in Neurosciences*, 34:515–525, 2011. doi:https://doi.org/10.1016/j.tins.2011.06.006, PMID: 21788086.

Adam Santoro. Reassessing pattern separation in the dentate gyrus. *Frontiers in Behavioral Neuroscience*, 7, 2013. ISSN 1662-5153. doi:10.3389/fnbeh.2013.00096.

Kenneth A. Norman and Randall C. O'Reilly. Modeling hippocampal and neocortical contributions to recognition memory: A complementary-learning-systems approach. *Psychological Review*, 110(4):611–646, 2003. doi:10.1037/0033-295X.110.4.611.

Inah Lee, D. Yoganarasimha, Geeta Rao, and James J. Knierim. Comparison of population coherence of place cells in hippocampal subfields ca1 and ca3. *Nature*, 430(6998):456–459, 2004. doi:10.1038/nature02739.

Segundo Jose Guzman, Alois Schlögl, Michael Frotscher, and Peter Jonas. Synaptic mechanisms of pattern completion in the hippocampal ca3 network. *Science*, 353(6304):1117–1123, 2016. doi:10.1126/science.aaf1836.

J. J. Hopfield. Neural networks and physical systems with emergent collective computational abilities. *Proceedings of the National Academy of Sciences of the United States of America*, 79(8):2554–2558, Apr 1982. doi:10.1073/pnas.79.8.2554.

Szabolcs Káli and Peter Dayan. The involvement of recurrent connections in area ca3 in establishing the properties of place fields: a model. *Journal of Neuroscience*, 20(19):7463–7477, 2000. ISSN 0270-6474. doi:10.1523/JNEUROSCI.20-19-07463.2000.

Edmund T. Rolls. *Memory, Attention, and Decision-Making: A Unifying Computational Neuroscience Approach*. Oxford University Press, 08 2007. ISBN 9780199232703. doi:10.1093/acprof:oso/9780199232703.001.0001.

César Rennó-Costa, John E. Lisman, and Paul F. M. J. Verschure. A signature of attractor dynamics in the ca3 region of the hippocampus. *PLOS Computational Biology*, 10(5):1–15, 05 2014. doi:10.1371/journal.pcbi.1003641.

Frank Raven and Sara J. Aton. The engram's dark horse: How interneurons regulate state-dependent memory processing and plasticity. *Frontiers in Neural Circuits*, 15:750541, 2021. doi:10.3389/fncir.2021.750541.

Kirstie A. Cummings, Anthony F. Lacagnina, and Roger L. Clem. Gabaergic microcircuitry of fear memory encoding. *Neurobiology of Learning and Memory*, 184:107504, 2021. ISSN 1074-7427. doi:https://doi.org/10.1016/j.nlm.2021.107504.

W. Martin Usrey, Michael P. Sceniak, and Barbara Chapman. Receptive fields and response properties of neurons in layer 4 of ferret visual cortex. *Journal of Neurophysiology*, 89(2):1003–1015, Feb 2003. doi:10.1152/jn.00749.2002.

Cristopher M. Niell and Michael P. Stryker. Highly selective receptive fields in mouse visual cortex. *Journal of Neuroscience*, 28(30):7520–7536, Jul 2008. doi:10.1523/JNEUROSCI.0623-08.2008.

Ling-yun Li, Xiaorui R. Xiong, Leena A. Ibrahim, Wei Yuan, Huizhong W. Tao, and Li I. Zhang. Differential Receptive Field Properties of Parvalbumin and Somatostatin Inhibitory Neurons in Mouse Auditory Cortex. *Cerebral Cortex*, 25(7):1782–1791, 01 2014. ISSN 1047-3211. doi:10.1093/cercor/bht417.

Adil G. Khan, Jasper Poort, Angus Chadwick, Antonin Blot, Maneesh Sahani, Thomas D. Mrsic-Flogel, and Sonja B. Hofer. Distinct learning-induced changes in stimulus selectivity and interactions of gabaergic interneuron classes in visual cortex. *Nature Neuroscience*, 21(6):851–859, May 2018. doi:10.1038/s41593-018-0143-z.

Yaël Perez, France Morin, and Jean-Claude Lacaille. A hebbian form of long-term potentiation dependent on mglur1a in hippocampal inhibitory interneurons. *Proceedings of the National Academy of Sciences*, 98(16):9401–9406, 2001. doi:10.1073/pnas.161493498.

Scott F. Owen, Sebnem N. Tuncdemir, Patrick L. Bader, Natasha N. Tirko, Gord Fishell, and Richard W. Tsien. Oxytocin enhances hippocampal spike transmission by modulating fast-spiking interneurons. *Nature*, 500(7463): 458–462, Aug 2013. doi:10.1038/nature12330.

Samuel M. Cohen, Huan Ma, Kishore V. Kuchibhotla, Brendon O. Watson, György Buzsáki, Robert C. Froemke, and Richard W. Tsien. Excitation-transcription coupling in parvalbumin-positive interneurons employs a novel cam kinase-dependent pathway distinct from excitatory neurons. *Neuron*, 90(2):292–307, Apr 2016. doi:10.1016/j.neuron.2016.03.001.

Tatiana Korotkova, Elke C. Fuchs, Alexey Ponomarenko, Jakob von Engelhardt, and Hannah Monyer. Nmda receptor ablation on parvalbumin-positive interneurons impairs hippocampal synchrony, spatial representations, and working memory. *Neuron*, 68(3):557–569, 2010. doi:10.1016/j.neuron.2010.09.017.

Xingzhi He, Jiarui Li, Guangjun Zhou, Hailan Hu, Shumin Duan, and Huan Ma. Gating of hippocampal rhythms and memory by synaptic plasticity in inhibitory interneurons. *Neuron*, 109(6):1013–1028.e9, March 2021. doi:10.1016/j.neuron.2021.01.014.

László Acsády, Anita Kamondi, Attila Sík, Tamás Freund, and György Buzsáki. Gabaergic cells are the major postsynaptic targets of mossy fibers in the rat hippocampus. *The Journal of Neuroscience*, 18(9):3386–3403, May 1998. doi:10.1523/JNEUROSCI.18-09-03386.1998.

Edmund Rolls. A quantitative theory of the functions of the hippocampal ca3 network in memory. *Frontiers in Cellular Neuroscience*, 7, 2013. ISSN 1662-5102. doi:10.3389/fncel.2013.00098.

Masako Tsukamoto, Takuya Yasui, Maki K. Yamada, Nobuyoshi Nishiyama, Norio Matsuki, and Yuji Ikegaya. Mossy fibre synaptic nmda receptors trigger non-hebbian long-term potentiation at entorhino-ca3 synapses in the rat. *The Journal of Physiology*, 546(Pt 3):665–675, Feb 2003. doi:10.1113/jphysiol.2002.033803.

David L. Hunt, Nagore Puente, Pedro Grandes, and Pablo E. Castillo. Bidirectional nmda receptor plasticity controls ca3 output and heterosynaptic metaplasticity. *Nature Neuroscience*, 16:1049–1059, 2013. doi:10.1038/nn.3461.

Thomas E Chater and Yukiko Goda. My neighbour hetero—deconstructing the mechanisms underlying heterosynaptic plasticity. *Current Opinion in Neurobiology*, 67:106–114, 2021. ISSN 0959-4388. doi:https://doi.org/10.1016/j.conb.2020.10.007.

Kyle R. Jenks, Katya Tsimring, Jacque Pak Kan Ip, Jose C. Zepeda, and Mriganka Sur. Heterosynaptic plasticity and the experience-dependent refinement of developing neuronal circuits. *Frontiers in Neural Circuits*, 15, 2021. ISSN 1662-5110. doi:10.3389/fncir.2021.803401.

Seiichiro Jinde, Veronika Zsiros, and Kazu Nakazawa. Hilar mossy cell circuitry controlling dentate granule cell excitability. *Frontiers in Neural Circuits*, 7:14, Feb 2013. doi:10.3389/fncir.2013.00014.

N. Alex Cayco-Gajic, Claudia Clopath, and R. Angus Silver. Sparse synaptic connectivity is required for decorrelation and pattern separation in feedforward networks. *Nature Communications*, 8(1):1116, Oct 2017. doi:10.1038/s41467-017-01109-y.

Thomas Hainmueller and Marlene Bartos. Dentate gyrus circuits for encoding, retrieval and discrimination of episodic memories. *Nature Reviews Neuroscience*, 21(3):153–168, Mar 2020. doi:10.1038/s41583-019-0260-z.

Eugene M. Izhikevich and Gerald M. Edelman. Large-scale model of mammalian thalamocortical systems. *Proceedings of the National Academy of Sciences of the United States of America*, 105(9):3593–3598, 2008. doi:10.1073/pnas.0712231105.

Michael E. Hasselmo and Chantal E. Stern. Theta rhythm and the encoding and retrieval of space and time. *NeuroImage*, 85(Pt 2):656–666, Jan 2014. doi:10.1016/j.neuroimage.2013.06.022.

Céline Drieu and Michaël Zugaro. Hippocampal sequences during exploration: Mechanisms and functions. *Frontiers in Cellular Neuroscience*, 13:232, Jun 2019. doi:10.3389/fncel.2019.00232.

Nora A. Herweg, Ethan A. Solomon, and Michael J. Kahana. Theta oscillations in human memory. *Trends in Cognitive Sciences*, 24(3):208–227, 2020. ISSN 1364-6613. doi:https://doi.org/10.1016/j.tics.2019.12.006.

A Bragin, G Jando, Z Nadasdy, J Hetke, K Wise, and G Buzsaki. Gamma (40-100 hz) oscillation in the hippocampus of the behaving rat. *Journal of Neuroscience*, 15(1):47–60, 1995. ISSN 0270-6474. doi:10.1523/JNEUROSCI.15-01-00047.1995.

Laura Lee Colgin. Rhythms of the hippocampal network. *Nature Reviews Neuroscience*, 17(4):239–249, Apr 2016. doi:10.1038/nrn.2016.21.

Vítor Lopes dos Santos, Gido M. van de Ven, Alexander Morley, Stéphanie Trouche, Natalia Campo-Urriza, and David Dupret. Parsing hippocampal theta oscillations by nested spectral components during spatial exploration and memory-guided behavior. *Neuron*, 100(4):940–952.e7, 2018. ISSN 0896-6273. doi:https://doi.org/10.1016/j.neuron.2018.09.031.

James E Kragel, Stephen VanHaerents, Jessica W Templer, Stephan Schuele, Joshua M Rosenow, Aneesha S Nilakantan, and Donna J Bridge. Hippocampal theta coordinates memory processing during visual exploration. *eLife*, 9:e52108, mar 2020. ISSN 2050-084X. doi:10.7554/eLife.52108.

Leila Reddy, Matthew W. Self, Benedikt Zoefel, Marlene Poncet, Jessy K. Possel, Judith C. Peters, Johannes C. Baayen, Sander Idema, Rufin VanRullen, and Pieter R. Roelfsema. Theta-phase dependent neuronal coding during sequence learning in human single neurons. *Nature Communications*, 12(1):4839, Aug 2021. doi:10.1038/s41467-021-25150-0.

Marije Ter Wal, Juan Linde-Domingo, Julia Lifanov, Frédéric Roux, Luca D. Kolibius, Stephanie Gollwitzer, Johannes Lang, Hajo Hamer, David Rollings, Vijay Sawlani, Ramesh Chelvarajah, Bernhard Staresina, Simon Hanslmayr, and Maria Wimber. Theta rhythmicity governs human behavior and hippocampal signals during memory-dependent tasks. *Nature Communications*, 12(1):7048, Dec 2021. doi:10.1038/s41467-021-27323-3.

Eric Lowet, Daniel J. Sheehan, Ulises Chialva, Rodrigo De Oliveira Pena, Rebecca A. Mount, Sheng Xiao, Samuel L. Zhou, Hua an Tseng, Howard Gritton, Sanaya Shroff, Krishnakanth Kondabolu, Cyrus Cheung, Yangyang Wang, Kiryl D. Piatkevich, Edward S. Boyden, Jerome Mertz, Michael E. Hasselmo, Horacio G. Rotstein, and Xue Han. Theta and gamma rhythmic coding through two spike output modes in the hippocampus during spatial navigation. *Cell Reports*, 42(8):112906, 2023. ISSN 2211-1247. doi:https://doi.org/10.1016/j.celrep.2023.112906.

Sandra Gattas, Myra Sarai Larson, Lilit Mnatsakanyan, Indranil Sen-Gupta, Sumeet Vadera, A. Lee Swindlehurst, Paul E. Rapp, Jack J. Lin, and Michael A. Yassa. Theta mediated dynamics of human hippocampal-neocortical learning systems in memory formation and retrieval. *Nature Communications*, 14(1):8505, Dec 2023. doi:10.1038/s41467-023-44011-6.

Gayle M. Wittenberg and Samuel S.-H. Wang. Malleability of spike-timing-dependent plasticity at the ca3–ca1 synapse. *The Journal of Neuroscience*, 26(24):6610–6617, Jun 2006. doi:10.1523/JNEUROSCI.5388-05.2006.

Rajiv K. Mishra, Sooyun Kim, Segundo J. Guzman, and Peter Jonas. Symmetric spike timing-dependent plasticity at ca3–ca3 synapses optimizes storage and recall in autoassociative networks. *Nature Communications*, 7(1):11552, May 2016. ISSN 2041-1723. doi:10.1038/ncomms11552.

Nelson Rebola, Mario Carta, and Christophe Mulle. Operation and plasticity of hippocampal ca3 circuits: implications for memory encoding. *Nature Reviews Neuroscience*, 18(4):208–220, Apr 2017. ISSN 1471-0048. doi:10.1038/nrn.2017.10.

András Ecker, Bence Bagi, Eszter Vértes, Orsolya Steinbach-Németh, Mária R Karlócai, Orsolya I Papp, István Miklós, Norbert Hájos, Tamás F Freund, Attila I Gulyás, and Szabolcs Káli. Hippocampal sharp wave-ripples and the associated sequence replay emerge from structured synaptic interactions in a network model of area ca3. *eLife*, 11:e71850, jan 2022. ISSN 2050-084X. doi:10.7554/eLife.71850.

Qing Cheng and Jerrel L. Yakel. The effect of 7 nicotinic receptor activation on glutamatergic transmission in the hippocampus. *Biochemical Pharmacology*, 97(4):439–444, 2015. ISSN 0006-2952. doi:https://doi.org/10.1016/j.bcp.2015.07.015.

Jennifer Robinson, Frédéric Manseau, Guillaume Ducharme, Bénédicte Amilhon, Erika Vigneault, Salah El Mestikawy, and Sylvain Williams. Optogenetic activation of septal glutamatergic neurons drive hippocampal theta rhythms. *Journal of Neuroscience*, 36(10):3016–3023, 2016. ISSN 0270-6474. doi:10.1523/JNEUROSCI.2141-15.2016.

Gunes Unal, Michael G. Crump, Tim J. Viney, Tímea Éltes, Linda Katona, Thomas Klausberger, and Peter Somogyi. Spatio-temporal specialization of gabaergic septo-hippocampal neurons for rhythmic network activity. *Brain Structure and Function*, 223(5):2409–2432, Jun 2018. doi:10.1007/s00429-018-1626-0.

Christina Müller and Stefan Remy. Septo-hippocampal interaction. *Cell and Tissue Research*, 373(3):565–575, Sep 2018. doi:10.1007/s00441-017-2745-2.

Angel Nuñez and Washington Buño. The theta rhythm of the hippocampus: From neuronal and circuit mechanisms to behavior. *Frontiers in Cellular Neuroscience*, 15, 2021. ISSN 1662-5102. doi:10.3389/fncel.2021.649262.

Tamara Gedankien, Ryan Joseph Tan, Salman Ehtesham Qasim, Haley Moore, David McDonagh, Joshua Jacobs, and Bradley Lega. Acetylcholine modulates the temporal dynamics of human theta oscillations during memory. *Nature Communications*, 14(1):5283, Aug 2023. doi:10.1038/s41467-023-41025-y.

Masahiro Mori, Beat H. Gähwiler, and Urs Gerber. Recruitment of an inhibitory hippocampal network after bursting in a single granule cell. *Proceedings of the National Academy of Sciences*, 104(18):7640–7645, 2007. doi:10.1073/pnas.0702164104.

Christine L. Torborg, Toshiaki Nakashiba, Susumu Tonegawa, and Chris J. McBain. Control of ca3 output by feedforward inhibition despite developmental changes in the excitation-inhibition balance. *The Journal of Neuroscience*, 30 (46):15628–15637, Nov 2010. doi:10.1523/JNEUROSCI.3099-10.2010.

Mario Treviño, Carmen Vivar, and Rafael Gutiérrez. Excitation-inhibition balance in the ca3 network–neuronal specificity and activity-dependent plasticity. *European Journal of Neuroscience*, 33(10):1771–1785, May 2011. doi:10.1111/j.1460-9568.2011.07670.x.

Kathleen E. Cosgrove, Emilio J. Galván, Stephen D. Meriney, and Germán Barrionuevo. Area ca3 interneurons receive two spatially segregated mossy fiber inputs. *Hippocampus*, 20(9):1003–1009, Sep 2010. doi:10.1002/hipo.20713.

Luke Y. Prince, Travis J. Bacon, Cezar M. Tigaret, and Jack R. Mellor. Neuromodulation of the feedforward dentate gyrus-ca3 microcircuit. *Frontiers in Synaptic Neuroscience*, 8:32, Oct 2016. doi:10.3389/fnsyn.2016.00032.

S. Ruediger, C. Vittori, E. Bednarek, and et al. Learning-related feedforward inhibitory connectivity growth required for memory precision. *Nature*, 473:514–518, 2011. doi:10.1038/nature09946.

Dano J. Morrison, Asim J. Rashid, Adelaide P. Yiu, Chen Yan, Paul W. Frankland, and Sheena A. Josselyn. Parvalbumin interneurons constrain the size of the lateral amygdala engram. *Neurobiology of Learning and Memory*, 135:91–99, 2016. ISSN 1074-7427. doi:https://doi.org/10.1016/j.nlm.2016.07.007.

Thomas Stefanelli, Cristina Bertollini, Christian Lüscher, Dominique Muller, and Pablo Mendez. Hippocampal somatostatin interneurons control the size of neuronal memory ensembles. *Neuron*, 89(5):1074–1085, 2016. ISSN 0896-6273. doi:https://doi.org/10.1016/j.neuron.2016.01.024.

Nannan Guo, Marta E Soden, Charlotte Herber, Michael TaeWoo Kim, Antoine Besnard, Paoyan Lin, Xiang Ma, Constance L Cepko, Larry S Zweifel, and Amar Sahay. Dentate granule cell recruitment of feedforward inhibition governs engram maintenance and remote memory generalization. *Nature Medicine*, 24(4):438–449, 2018. doi:10.1038/nm.4491.

Silvia Viana da Silva, Pei Zhang, Matthias Georg Haberl, Virginie Labrousse, Noëlle Grosjean, Christophe Blanchet, Andreas Frick, and Christophe Mulle. Hippocampal mossy fibers synapses in ca3 pyramidal cells are altered at an early stage in a mouse model of alzheimer's disease. *J Neurosci*, 39(21):4193–4205, 2019. doi:10.1523/JNEUROSCI.2868-18.2019.

Corinna Giorgi and Silvia Marinelli. Roles and transcriptional responses of inhibitory neurons in learning and memory. *Frontiers in Molecular Neuroscience*, 14, 2021. ISSN 1662-5099. doi:10.3389/fnmol.2021.689952.

Catherine E. Myers and Helen E. Scharfman. A role for hilar cells in pattern separation in the dentate gyrus: a computational approach. *Hippocampus*, 19(4):321–337, Apr 2009. doi:10.1002/hipo.20516.

Faramarz Faghihi and Ahmed A. Moustafa. A computational model of pattern separation efficiency in the dentate gyrus with implications in schizophrenia. *Frontiers in Systems Neuroscience*, 9:42, Mar 2015. doi:10.3389/fnsys.2015.00042.

Spyridon Chavlis, Panagiotis C. Petrantonakis, and Panayiota Poirazi. Dendrites of dentate gyrus granule cells contribute to pattern separation by controlling sparsity. *Hippocampus*, 27(1):89–110, Jan 2017. doi:10.1002/hipo.22675.

Antoine D. Madar, Laura A. Ewell, and Mathew V. Jones. Pattern separation of spiketrains in hippocampal neurons. *Scientific Reports*, 9:5282, Mar 2019. doi:10.1038/s41598-019-41766-9.

Nazal Modhej, Azam Bastanfard, Mohammad Teshnehlab, and Somayeh Raiesdana. Pattern separation network based on the hippocampus activity for handwritten recognition. *IEEE Access*, 8:212803–212817, 2020. doi:10.1109/ACCESS.2020.3040298.

S. Jose Guzman, Alois Schlögl, Claudia Espinoza, Xiaomin Zhang, Benjamin A. Suter, and Peter Jonas. How connectivity rules and synaptic properties shape the efficacy of pattern separation in the entorhinal cortex–dentate gyrus–ca3 network. *Nature Computational Science*, 1(12):830–842, 2021. doi:10.1038/s43588-021-00157-1.

Sang-Yoon Kim and Woochang Lim. Disynaptic effect of hilar cells on pattern separation in a spiking neural network of hippocampal dentate gyrus. *Cognitive Neurodynamics*, 16(6):1427–1447, Dec 2022. doi:10.1007/s11571-022-09797-z.

Tamás F. Freund and György Buzsáki. Interneurons of the hippocampus. *Hippocampus*, 6(4):347–470, 1996. doi:10.1002/(SICI)1098-1063(1996)6:4<347::AID-HIPO1>3.0.CO;2-I.

David G. Amaral, Helen E. Scharfman, and Pierre Lavenex. The dentate gyrus: fundamental neuroanatomical organization (dentate gyrus for dummies). *Progress in Brain Research*, 163:3–22, 2007. doi:10.1016/S0079-6123(07)63001-5.

Nathan B. Danielson, Gergely F. Turi, Max Ladow, Spyridon Chavlis, Panagiotis C. Petrantonakis, Panayiota Poirazi, and Attila Losonczy. In vivo imaging of dentate gyrus mossy cells in behaving mice. *Neuron*, 93(3):552–559.e4, 2017. ISSN 0896-6273. doi:https://doi.org/10.1016/j.neuron.2016.12.019.

Hubert Löffler and Daya Shankar Gupta. A model of pattern separation by single neurons. *Frontiers in Computational Neuroscience*, 16, 2022. ISSN 1662-5188. doi:10.3389/fncom.2022.858353.

Tristan J. Webb, Edmund T. Rolls, Gustavo Deco, and Jianfeng Feng. Noise in attractor networks in the brain produced by graded firing rate representations. *PLOS ONE*, 6(9):1–15, 09 2011. doi:10.1371/journal.pone.0023630.

Endel Tulving and Donald M. Thomson. Encoding specificity and retrieval processes in episodic memory. *Psychological Review*, 80(5):352–373, 1973. doi:10.1037/h0020071.

Linou Ji. The validity of the specific coding principle: the explanations from cognitive psychology and psychoanalysis. *Journal of Education, Humanities and Social Sciences*, 8:1259–1263, Feb. 2023. doi:10.54097/ehss.v8i.4460.

Gustavo Deco and Edmund T. Rolls. Decision-making and weber's law: a neurophysiological model. *European Journal of Neuroscience*, 24(3):901–916, 2006. doi:https://doi.org/10.1111/j.1460-9568.2006.04940.x.

Michael Watkins and Olga Watkins. Cue-overload theory and the method of interpolated attributes. *Bulletin of the Psychonomic Society*, 7:289–291, 03 2013. doi:10.3758/BF03337192.

Alan Parkin. Levels of processing and the cue overload principle. *Quarterly Journal of Experimental Psychology - QUART J EXP PSYCHOL*, 32:427–434, 05 2007. doi:10.1080/14640748008401836.

Joshua P. Neunuebel and James J. Knierim. Ca3 retrieves coherent representations from degraded input: direct evidence for ca3 pattern completion and dentate gyrus pattern separation. *Neuron*, 81(2):416–427, 2014. doi:10.1016/j.neuron.2013.11.017.

Stefan Leutgeb, Jill K. Leutgeb, Alessandro Treves, May-Britt Moser, and Edvard I. Moser. Distinct ensemble codes in hippocampal areas ca3 and ca1. *Science*, 305(5688):1295–1298, 2004. doi:10.1126/science.1100265.

John F. Guzowski, James J. Knierim, and Edvard I. Moser. Ensemble dynamics of hippocampal regions ca3 and ca1. *Neuron*, 44(4):581–584, 2004. ISSN 0896-6273. doi:https://doi.org/10.1016/j.neuron.2004.11.003.

Joe Guillaume Pelletier and Jean-Claude Lacaille. Chapter 14 long-term synaptic plasticity in hippocampal feedback inhibitory networks. In Wayne S. Sossin, Jean-Claude Lacaille, Vincent F. Castellucci, and Sylvie Belleville, editors, *Essence of Memory*, volume 169 of *Progress in Brain Research*, pages 241–250. Elsevier, 2008. doi:https://doi.org/10.1016/S0079-6123(07)00014-3.

Meryl Malezieux, Ashley L. Kees, and Christophe Mulle. Theta oscillations coincide with sustained hyperpolarization in ca3 pyramidal cells, underlying decreased firing. *Cell Reports*, 32(1):107868, 2020. ISSN 2211-1247. doi:https://doi.org/10.1016/j.celrep.2020.107868.

Edvard I Moser and May-Britt Moser. One-shot memory in hippocampal ca3 networks. *Neuron*, 38(2):147–148, 2003. ISSN 0896-6273. doi:https://doi.org/10.1016/S0896-6273(03)00227-7.

Sang Wan Lee, John P. O'Doherty, and Shinsuke Shimojo. Neural computations mediating one-shot learning in the human brain. *PLOS Biology*, 13(4):1–36, 04 2015. doi:10.1371/journal.pbio.1002137.

Zhenrui Liao and Attila Losonczy. Learning, fast and slow: Single- and many-shot learning in the hippocampus. *Annual Review of Neuroscience*, April 2024. doi:10.1146/annurev-neuro-102423-100258.

Alejandro Javier Pernía-Andrade and Peter Jonas. Theta-gamma-modulated synaptic currents in hippocampal granule cells in vivo define a mechanism for network oscillations. *Neuron*, 81(1):140–152, 2014. ISSN 0896-6273. doi:https://doi.org/10.1016/j.neuron.2013.09.046.

Arjun V. Masurkar. Towards a circuit-level understanding of hippocampal ca1 dysfunction in alzheimer's disease across anatomical axes. *Journal of Alzheimer's Disease & Parkinsonism*, 8(1):412, Jan 2018. doi:10.4172/2161-0460.1000412.

Nuri Jeong and Annabelle C. Singer. Learning from inhibition: Functional roles of hippocampal ca1 inhibition in spatial learning and memory. *Current Opinion in Neurobiology*, 76:102604, 2022. ISSN 0959-4388. doi:https://doi.org/10.1016/j.conb.2022.102604.

John Bickle. The first two decades of creb-memory research: data for philosophy of neuroscience. *AIMS Neuroscience*, 8(3):322–339, February 2021. doi:10.3934/Neuroscience.2021017.

Yanqing Chen. Mechanisms of winner-take-all and group selection in neuronal spiking networks. *Frontiers in Computational Neuroscience*, 11, 2017. ISSN 1662-5188. doi:10.3389/fncom.2017.00020.

Yanqing Chen, Jeffrey L. Mckinstry, and Gerald M. Edelman. Versatile networks of simulated spiking neurons displaying winner-take-all behavior. *Frontiers in Computational Neuroscience*, 7, 2013. ISSN 1662-5188. doi:10.3389/fncom.2013.00016.

K. Chen and L. Wang. *Trends in Neural Computation*, volume 1 of *Studies in Computational Intelligence*. Springer Nature, United States, 1 edition, 2007.